Catalysis Science & Technology

ROYAL SOCIETY OF CHEMISTRY

REVIEW

View Article Online
View Journal | View Issue

Cite this: *Catal. Sci. Technol.*, 2024, 14, 6466

Enhancing light-driven photocatalytic reactions through solid solutions of bismuth oxyhalide/bismuth rich photocatalysts: a systematic review

Robert O. Gembo,[a] Rudzani Ratshiedana,[a] Lawrence M. Madikizela,[a] Ilunga Kamika,[a] Cecil K. King'ondu,[b] Alex T. Kuvarega[a] and Titus A. M. Msagati *[a]

The pursuit of sustainable environmental remediation strategies has led to intensive research in photocatalysis. Photocatalysts are a class of compounds with exceptional properties, making them suitable for various applications in environmental remediation. They are effective against multiple organic and inorganic pollutants and are also used as semiconductors for green energy production. Among the various photocatalytic semiconductor materials explored, bismuth oxyhalide (BiOY, Y = F, Cl, Br, or I) and bismuth-rich ($Bi_xO_yY_z$, Y = F, Cl, Br, or I) are particularly notable. However, unmodified/pristine BiOY and $Bi_xO_yY_z$ exhibit inherent limitations of low photocatalytic performance owing to unsuitable band gaps and low efficiency in separating carriers. Hence, this review outlines the BiOY and $Bi_xO_yY_z$ structures, wherein modifiable halogen layers may offer favorable conditions for creating solid solutions with improved intrinsic properties and catalytic performance. This systematic review also explores the unique attributes and challenges associated with tuning the photocatalytic performance of BiOY and $Bi_xO_yY_z$ solid solutions to enhance solar-driven reactions. The distinctive feature of this review lies in the versatile nature of the BiOY and $Bi_xO_yY_z$ solid solution materials. These materials offer the advantage of harnessing a broad light spectrum, including solar and UV radiation. This review further explores the strategies and techniques employed to optimize BiOY and $Bi_xO_yY_z$ photocatalysts by forming solid solution and their application in water treatment processes. Furthermore, it highlights the ongoing challenges and opportunities in developing high-performance BiOY and $Bi_xO_yY_z$ solid solution photocatalysts, illustrating their potential to drive a more sustainable and energy-efficient future through enhanced light-driven reactions.

Received 2nd July 2024,
Accepted 1st October 2024

DOI: 10.1039/d4cy00820k

rsc.li/catalysis

1. Introduction

The worldwide population explosion, technological advancement increase, environmental degradation, and rising energy requirements have presented humanity with profound challenges, including energy deficits, ecological contamination, and climate change.[1] Environmental contamination resulting from volatile organic compounds, heavy metals, polymer residues, microplastics, and biological pollutants has become a substantial socioeconomic issue stemming from industrialization and urbanization.[2,3] Ecosystem function and public health may be profoundly imperiled by the presence of organic xenobiotics in the environment, which can be very harmful, even at trace concentrations. These organic compounds cannot be completely removed from environmental matrices *via* conventional contaminant remediation methodologies, such as filtration, precipitation, adsorption, and centrifugation. These methods transform these organic compounds into solid sludge rather than breaking them entirely.[4]

On the other hand, the finite reserves of carbonaceous fossil fuel feedstocks are being rapidly depleted due to the continuous growth of the global human population, rendering energy production one of the preeminent challenges that humanity will confront in the proximate future. Consequently, the paramount issue of how to employ scientific methodologies to resolve these multifaceted issues and ensure the sustainable development of human civilization emerges. The exploration and harnessing of sustainable, renewable energy modalities, such as wind, tidal, solar power, and ocean thermal, garner substantial interest and investment. Therefore, developing efficient and environmentally benign techniques and technologies is paramount. Renewable energy sources should power these methods and aim to transform harmful contaminants into harmless substances without causing secondary pollution.[5]

Among the most valuable gifts bestowed by nature is the abundant and clean source of solar light that stands out as

[a] *Institute for Nanotechnology and Water Sustainability, College of Science, Engineering and Technology, University of South Africa, Florida 1709, Roodepoort, Johannesburg, South Africa. E-mail: msagatam@unisa.a.za*
[b] *Department of Chemical and Forensic Sciences, Botswana International University of Science and Technology, Palapye, Botswana*

an unparalleled source of thermal and non-thermal energy. Semiconductor photocatalysis, a viable technology for harnessing solar energy, holds immense promise for various applications, including environmental remediation, energy generation, organic synthesis, and medical treatments.[6] The field of semiconductor photocatalysis was inaugurated by pioneering studies conducted in 1972, which demonstrated the process of photolytic water decomposition using titanium dioxide (TiO_2) anodes under ultraviolet illumination.[7] Since then, this field has entered a substantial growth phase marked by significant advancements in developing efficient photocatalysts. Notably, a variety of materials, such as metallic oxides (*e.g.*, TiO_2, ZnO, Ta_2O_5, Fe_2O_3), nitrides (*e.g.*, Ta_3N_5, TaON), and sulfides (*e.g.*, CdS, MoS_2), have been extensively studied and explored for their photocatalytic properties.[8–11]

To date, this has sparked widespread enthusiasm for intensive exploration in developing high-performance semiconductor photocatalysts, aiming to mitigate the energy crisis and address environmental challenges. Bismuth-based photocatalysts with layered structures have attracted substantial research attention in photocatalysis. This heightened interest stems from their distinctive characteristics, including a layered crystal structure, diverse compositions, intricate atomic coordination, and an enticing hybrid electronic band structure. These qualities provide a versatile platform for crystal structure design, control over morphology and facets, band structure regulation, defect formation, and a host of other modifications to enhance solar energy conversion efficiency.[12,13]

Some reviews have documented the use of bismuth-based photocatalysts in diverse photocatalytic light-driven processes.[14–21] These reviews have detailed various modification methodologies, including oxygen vacancies[14,15] ternary nanocomposites[16,17] manipulation of crystal vacancy defects,[18] establishment of heterojunctions, employing sensitizers, consideration of facet effects, regulation of microstructure, incorporation of surface plasmonic resonance, implementation of strain engineering, control of morphology, and elemental doping.[19–21] However, to the best of our knowledge, there is no reported review dedicated exclusively to the tuning/modification of BiOY and $Bi_xO_yY_z$ photocatalyst materials through the formation of solid solutions. Therefore, this review highlights enhancing BiOY and $Bi_xO_yY_z$ photocatalysts through solid solution tuning for better practical use in diverse photocatalytic processes, exploring structural customization's impact on efficacy. In addition, it reports the strategies for improving the intrinsic properties of BiOY and $Bi_xO_yY_z$ solid solutions. Furthermore, it highlights the ongoing challenges and opportunities in the quest for high-performance photocatalysts, illustrating their potential to drive a more sustainable and energy-efficient future through enhanced light-driven reactions (LDR).

1.1. Structures of BiOY and $Bi_xO_yY_z$ materials

Several diverse bismuth-based photocatalysts including bismuth oxyhalides (BiOY),[22] bismuth vanadate ($BiVO_4$),[23] bismuth titanates ($Bi_xTi_yO_z$),[24] bismuth tungstate (Bi_2WO_6),[25] bismuth oxycarbonates ($Bi_2O_2CO_3$),[26] bismuth silicates ($Bi_xSi_yO_z$),[27] bismuth ferrites ($BiFeO_3$),[28] bismuth molybdates (Bi_2MoO_6),[29] bismuth iodates ($Bi(IO_3)_3$),[30] bismuth niobites ($BiNbO_4$),[31] bismuth phosphate ($BiPO_4$),[32] have been fabricated. This range of materials benefits from the orbital hybridization between Bi 6s in Bi(III) and O 2p, resulting in a broader hybridized state. This, in turn, yields a narrower bandgap for improved photoabsorption and highly dispersive band structures, facilitating rapid charge migration.[33,34] Bismuth oxyhalide, a remarkable photocatalyst with a layered structure containing [Y–Bi–O–Bi–Y] slabs interspersed by dual-halogen atom slabs, is a Bi-based photocatalyst that has gained significant attention globally.[35]

Several notable and intriguing findings have emerged from studies on BiOY photocatalysts. The internal static electric field within this multilayered structure (BiOY photocatalysts) has been found to facilitate the separation of electron–hole pairs, thereby enhancing photocatalytic performance.[2829] The layers composed of [Y–Bi–O–Bi–Y] joined by van der Waals forces to create a tetragonal matlockite crystal lattice,[36] as illustrated in Fig. 1. Historically, BiOY substances have been used extensively as storage and ferroelectric materials, catalysts, and pigments. Nevertheless, in recent years, novel applications have been discovered across diverse domains, encompassing CO_2 photoreduction,[37–39] photocatalytic cleansing of wastewater,[40–43] water splitting,[44] alcohol oxidation, and organic synthesis.[45–47]

The considerable charge transfer dynamics resulting from the indirect bandgap characteristics of these semiconductors, in conjunction with their well-defined crystalline structures, render these materials highly promising candidates for H_2 production applications. Furthermore, the induction of a perpendicular internal electric field across the (001) crystallographic plane of BiOY photocatalysts can facilitate enhanced charge carrier separation along this preferred orientation.[48] A key advantage of BiOY materials is their broad range of tunable bandgap energies, spanning from 3.3 eV for BiOCl to 1.8 eV for BiOI. This wide bandgap tunability enables the utilization of these photocatalysts under visible light illumination.[49,50] Since Zhang *et al.* 2006 (ref. 51) documented the production of three-dimensional microspheres consisting of BiOY on two-dimensional nanoplates using solvothermal synthesis to degrade methyl orange, many researchers have focused on investigating the photocatalytic capabilities of BiOY materials.[43,52–56]

1.2. Properties of BiOY and $Bi_xO_yY_z$ materials

Compared to the BiOY class of photocatalysts, the $Bi_xO_yY_z$ materials also exhibit a layered crystal structure characterized by robust interlayer covalent bonding and weak interlayer non-bonding van der Waals interactions. Taking $Bi_4O_5Br_2$ as an illustrative example, Fig. 2 provides a schematic representation of the crystallographic arrangement of this representative $Bi_xO_yY_z$ compound. The crystal structure of $Bi_4O_5Br_2$ is composed of [Bi–O] layers

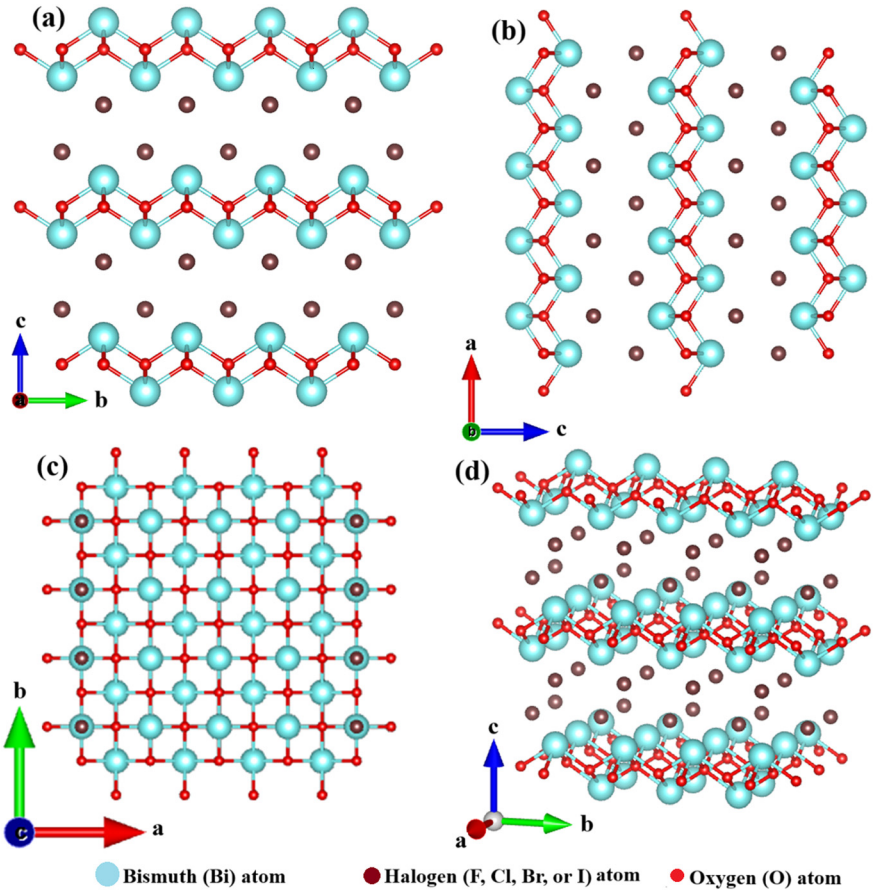

Fig. 1 Structure of BiOY systems featuring Y–Bi–O–Bi–Y slabs arranged in a stoichiometric manner along the (a) *a*, (b) *b*, (c) *c*-axis, and (d) standard orientation of crystal shape.

positioned between two bromine ion slabs, resulting in a distinctly layered architectural motif. Interestingly, the charge density surrounding the [Bi–O] layers is found to be greater than that of the adjacent double bromine slabs in the $Bi_4O_5Br_2$ structure. This non-uniform charge distribution between the [Bi–O] and double bromine layers induces a static internal electric field (IEF) within the material, which can facilitate the efficient separation of photogenerated electron–hole pairs.[57–59]

The directional growth of the layered $Bi_4O_5Br_2$ aligns with the [101] direction, leading to an internal electric field direction in the [101] orientation, which deviates from the [001] direction observed in BiOY. Density functional theory (DFT) calculations and empirical findings have consistently demonstrated the increased photon absorption efficiency of $Bi_xO_yY_z$. This observation was corroborated by previous studies.[60,61] Facilitating charge carrier separation efficiency is a critical factor in optimizing the performance of semiconductor-based photocatalytic systems. In the case of $Bi_xO_yY_z$ photocatalysts, the primary mechanism driving the efficacy of charge separation is the intrinsic internal electric field situated between its distinctive layered structural layers.[57]

Generally, for semiconductor-based photocatalytic systems, increased internal electric field intensity typically corresponds to enhanced efficiency in the spatial separation of photogenerated charge carriers. The strength of this internal electric field is determined by the magnitude of the polarization space and the material's polarization force. The substantial interlayer spacing and pronounced dipole moment characteristics inherent to the layered $Bi_xO_yY_z$ crystal structure contribute to these materials' improved polarization space and polarization force. Furthermore, increasing the ratio of Bi to the halogen element (X) not only boosts the optical absorption capabilities but also fortifies the hybridization of the conduction band, thereby facilitating electron migration and promoting the spatial separation of photogenerated electron–hole pairs.[58] As a result of these advantageous structural and electronic features, the $Bi_xO_yY_z$ class of photocatalytic materials has demonstrated outstanding performance in a wide range of applications. Since the initial report of Bi_3O_4Cl photocatalysts by Lin *et al.*[62] in 2006, a series of additional $Bi_xO_yY_z$ photocatalysts, including $Bi_{24}O_{31}Cl_{10}$, $Bi_{12}O_{17}Cl_2$, $Bi_{12}O_{15}Cl_6$, Bi_3O_4Cl, Bi_3O_4Br, $Bi_{12}O_{17}Br_2$, $Bi_{24}O_{31}Br_{10}$, $Bi_4O_5Br_2$, Bi_5O_7Br, $Bi_4O_5I_2$, $Bi_7O_9I_3$, and Bi_5O_7I, have been extensively studied and documented in the review by Jin *et al.*[63] The tunable bandgap energies of $Bi_xO_yY_z$ nanocrystals, spanning from 2.0 to 3.6 eV, enable their efficient utilization under a broad range of illumination conditions, including the UV-visible light spectrum.[63] However, further improvements in the properties and performance of both BiOY and $Bi_xO_yY_z$ photocatalyst

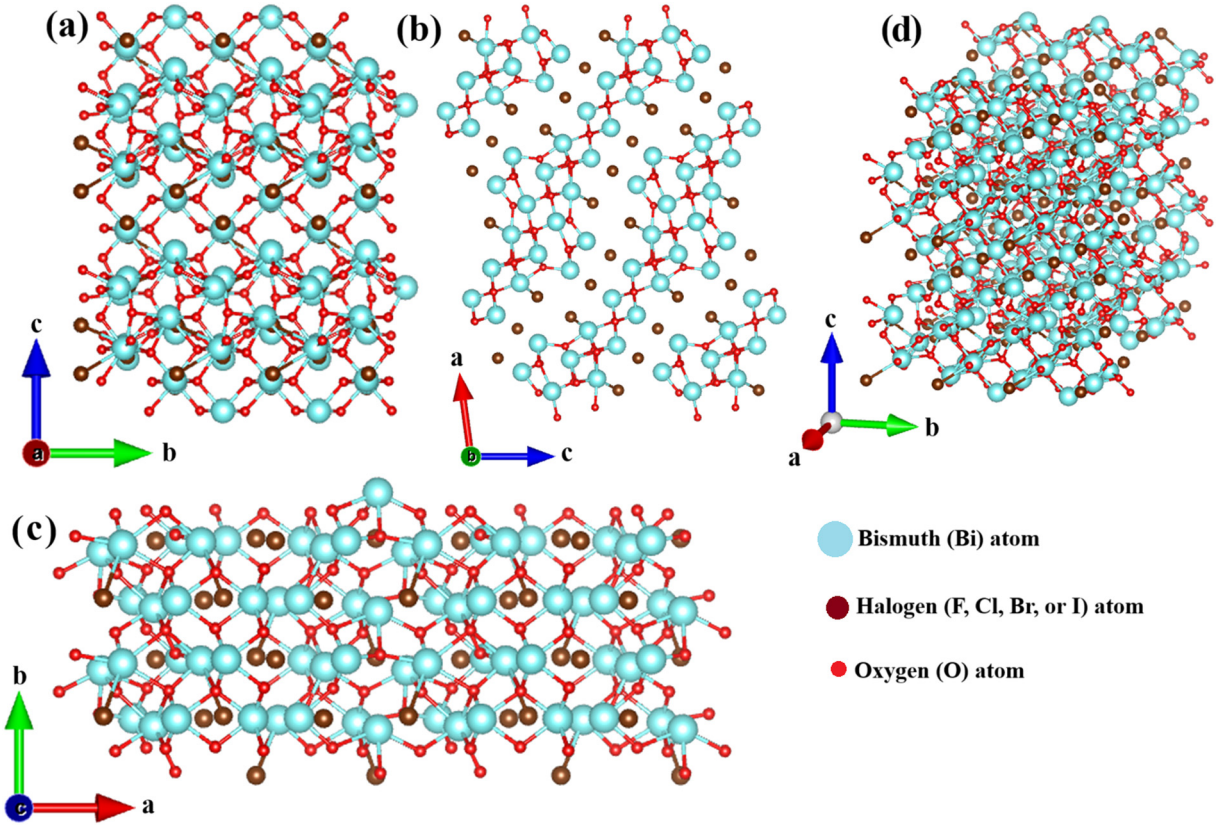

Fig. 2 The structural model of $Bi_4O_5Br_2$ along (a) *a*, (b) *b*, (c) *c*-axis, and (d) standard orientation of crystal shape.

materials will be necessary to facilitate their widespread commercial and industrial adoption.

2. Fabrication of BiOY and $Bi_xO_yY_z$ photocatalytic material

The methodologies employed for synthesis significantly contribute to the effective fabrication of nano- and micro-structures in accordance with specific requirements. The pivotal factors governing the production of BiOY nanomaterials are enhanced through facile synthesis. Recently, several techniques have been established for the synthesis of BiOY and its composites by using hydrolysis, hydrothermal, ion exchange, co-precipitation, deposition–precipitation, photodeposition, thermal reduction, direct combination, electrostatic self-assembly, template-assisted, and microwave-assisted methods.[64] As advancements in traditional BiOY continue, bismuth-rich and oxyhalides

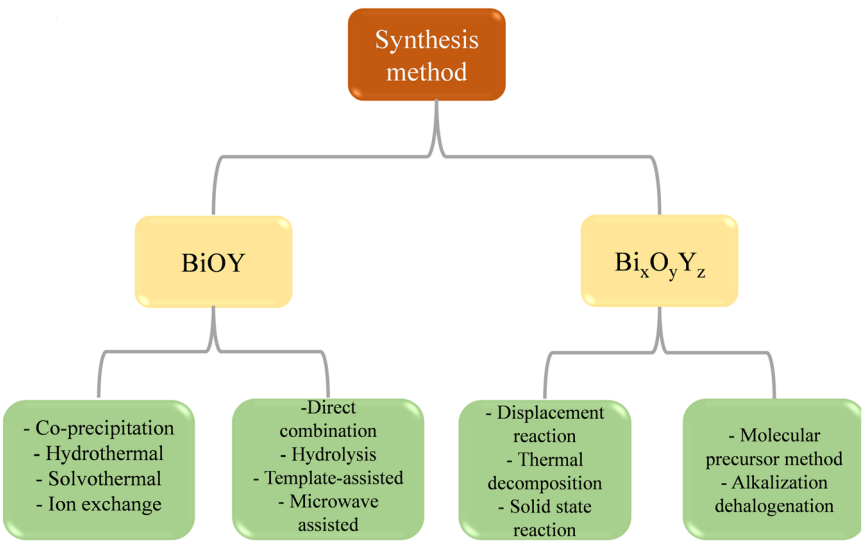

Fig. 3 Various synthetic techniques to produce BiOY and Bi-rich $Bi_xO_yY_z$ materials.

exhibit discernible differences in local atomic structure, electronic configuration, optical properties, and electrical conductivity compared to BiOY. Consequently, the physicochemical attributes and photocatalytic behavior can be effectively tailored. Given this context, it is crucial to summarize[65–67] effective strategies for the controlled synthesis of $Bi_xO_yY_z$ and delve into the intrinsic mechanisms governing its formation processes. The preparation of $Bi_xO_yY_z$ materials through a high-temperature solid-state reaction is straightforward. This process involves combining precursors with specific elemental stoichiometric ratios subjected to elevated temperatures to yield the desired components of $Bi_xO_yY_z$, as shown in Fig. 3. For instance, the synthesis of Bi_3O_4Cl entails blending Bi_2O_3 and BiOCl powders in a stoichiometric proportion, followed by calcination at 700 °C in an air environment for 24 h.[62]

3. Recent advances in characterization techniques

Significant progress has been made in characterization approaches for BiOY and $Bi_xO_yY_z$ materials in recent studies, especially in understanding their structural, electrical, and catalytic properties. These materials are becoming more and more popular because of their possible uses in electrical devices, photocatalysis, and energy storage.[21] The combination of machine learning and conventional characterization methods, such as X-ray absorption spectroscopy, is one of the major developments. By speeding up the study of sophisticated materials like BiOY and $Bi_xO_yY_z$, this method makes it possible to forecast chemical speciation and electrical structure with more accuracy-predictions that are essential for maximizing the material's performance in a variety of applications.[63]

Furthermore, studies have concentrated on the synthesis and mechanistic comprehension of these substances, particularly concerning their stability and effectiveness in energy-related uses. For example, new synthesis techniques and sophisticated characterization instruments are being used to produce materials that are more stable in real-world settings. Applications in hydrogen storage and transformation, where the stability and effectiveness of materials like BiOY and BiOY and $Bi_xO_yY_z$ are crucial, demand for this in particular.[68] Overall, the practical application of BiOY and $Bi_xO_yY_z$ materials in next-generation technologies is being made possible by the combination of cutting-edge characterization techniques and creative synthesis approaches.

Structural characterization is achieved through X-ray diffraction (XRD), which provides insights into crystallite size and phase purity, while scanning electron microscopy (SEM) and transmission electron microscopy (TEM) reveal surface and internal morphology, respectively. Compositional analysis is performed using energy dispersive X-ray spectroscopy (EDS/EDX) and X-ray photoelectron spectroscopy (XPS), which detail elemental composition and surface chemical states. Raman spectroscopy (RS) and Fourier transform infrared spectroscopy (FTIR) offer information on bonding and molecular vibrations. Optical and electronic properties are explored with UV-visible spectroscopy and electrical conductivity measurements. Finally, Brunauer–Emmett–Teller (BET) surface area analysis and thermogravimetric nalysis (TGA) assess surface area and thermal stability, respectively. These techniques collectively provide a comprehensive understanding of the materials' characteristics, as summarized in Fig. 4.

4. BiOY and $Bi_xO_yY_z$ modification strategies

The photon absorption efficiency and carrier separation are critical challenges for semiconductor photocatalysts. Despite the strong visible-light photocatalytic properties exhibited by BiOY and $Bi_xO_yY_z$ materials, their practical application is hindered by their low overall photocatalytic efficiency, primarily attributed to photo-induced carriers' rapid recombination.

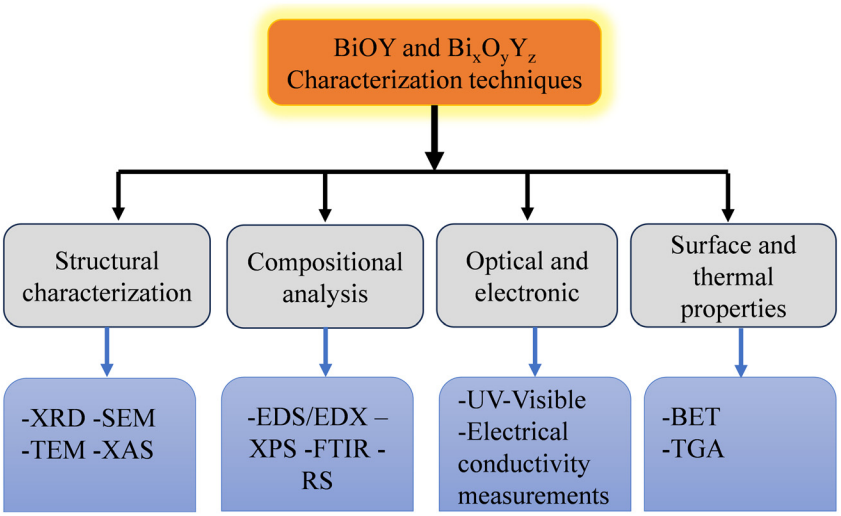

Fig. 4 Overview of characterization techniques for BiOY and $Bi_xO_yY_z$ compounds.

Additionally, three common types of BiOY (BiOCl, BiOBr, and BiOI) respond differently to visible light. Therefore, to optimize the solar energy utilization of BiOY and $Bi_xO_yY_z$ in various photocatalytic light-driven processes, photocatalysts must exhibit a robust response to visible light, which constitutes a higher percentage of solar irradiation. This photocatalytic enhancement has been achieved through various modification strategies, such as coupling, doping, cocatalyst usage, and solid solutions, to improve charge separation.[63,69]

Various strategies, as depicted in Fig. 5, have been comprehensively reported in different reviews.[14–21] Creating solid solutions is a promising avenue among the various strategies explored to enhance the properties of BiOY and Bi_xOY_z photocatalysts. Therefore, the present review provides a novel contribution to the current body of knowledge by elucidating the intricate details of solid solutions. This topic has yet to be extensively explored in existing literature. This review exclusively reports methods used to enhance the photocatalytic performance of BiOY and $Bi_xO_yY_z$ solid solutions materials and their application in the degradation of various water contaminants.

4.1. Solid solutions

Solid solutions, which are homogeneous crystalline structures formed by the dissolution of two or more crystalline phases, can be created under solid-state conditions and using wet chemistry methods. Unlike a mere physical mixture of solid powders, a solid solution retains a singular phase, with constituent elements hybridizing at the atomic level. The structures and properties of these solid solutions can be altered by varying their constituent components, offering the potential for tailored electronic properties. For example, in certain cases, the band gap of a solid solution can be narrower than that of the individual components, making them highly attractive for applications requiring precise electronic characteristics.[70] Solid solutions have been successfully applied across various domains, serving as electrocatalysts and photocatalysts with exceptional activity, selectivity, and stability as catalyst substrates. Examples include well-known materials like gallium arsenide (GaAs), gallium phosphide (GaP), aluminum arsenide (AlAs), and indium arsenide (InAs), where the selection of component solids is based on the desired characteristics of the resulting solid solution.[71]

In the field of photocatalysis, the construction of solid solutions from bismuth oxyhalides (BiOX, where X = Cl, Br, and I) and bismuth-rich compounds ($Bi_xO_yY_z$) has garnered significant attention. The halogen atoms in BiOX vary, leading to unique band gaps in these materials. By producing solid solutions, such as $BiOCl_xBr_y$ and $BiOBr_xI_y$, the band gaps can be precisely controlled to absorb a broader range of the solar spectrum, particularly extending into the visible light region. This redshifting of the absorption edge, which occurs when halides are mixed, enables the photocatalyst to harness more visible light, a crucial factor for solar-powered applications like pollution degradation and water splitting.[72,73]

The photocatalytic activity of these solid solutions can be finely tuned by adjusting the ratios of the Cl^-, Br^-, and I^- ion components. BiOY (where Y = Cl, Br, I) displays different photo responses due to the distinct band gaps of BiOCl (3.3 eV), BiOBr (2.7 eV), and BiOI (1.8 eV). Because of their similar structural characteristics and atomic arrangements, Y can be arbitrarily adjusted to form BiOX–BiOY (X, Y = Cl, Br, I, and X + Y = 1) solid solutions (Fig. 6a), allowing for precise regulation of the photo response and optimizing the photocatalytic activity.[74] This construction of solid solutions from BiOY and $Bi_xO_yY_z$ has garnered considerable attention over the years, as shown in Fig. 6b.[74]

Moreover, solid solutions offer a multidimensional strategy for enhancing photocatalytic performance by adjusting band gaps, improving charge carrier dynamics, introducing beneficial imperfections, and increasing structural stability. The creation of heterojunctions within solid solutions, which serve as recombination barriers, facilitates the separation of photogenerated electron–hole pairs, thereby increasing the efficiency of photocatalytic reactions.[75] These advantages make solid solutions a robust and adaptable platform for photocatalysis, particularly in applications where high efficiency and long-term stability under sunlight are essential.[76]

4.1.1. Bismuth oxyhalide solid solution. Recent progress in solid solution synthesis represents a substantial advancement in bandgap engineering, facilitating the customization of compounds to enhance the sensitization of photocatalysts in the visible light region. This engineering achievement allows for the narrowing of the bandgaps by either lowering the conduction band (CB) level or raising the valence band (VB) level.[77] For instance, BiOY solid solutions involve the partial

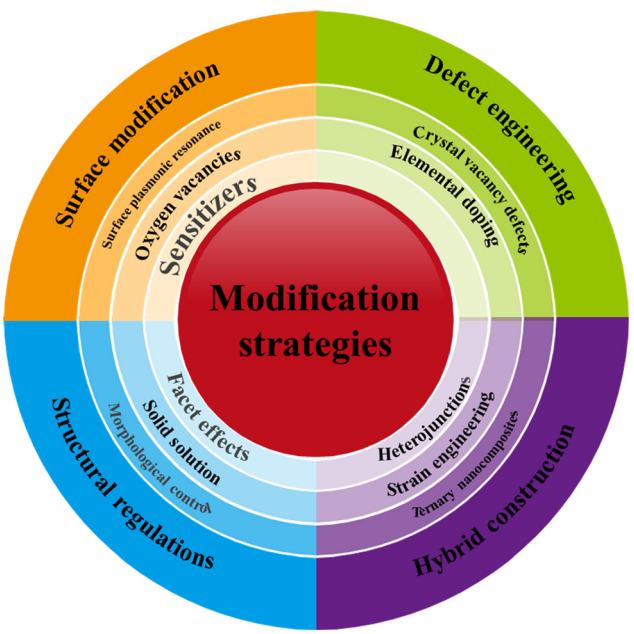

Fig. 5 Classification of proposed tuning strategies for BiOY and Bi-rich $Bi_xO_yY_z$ materials.

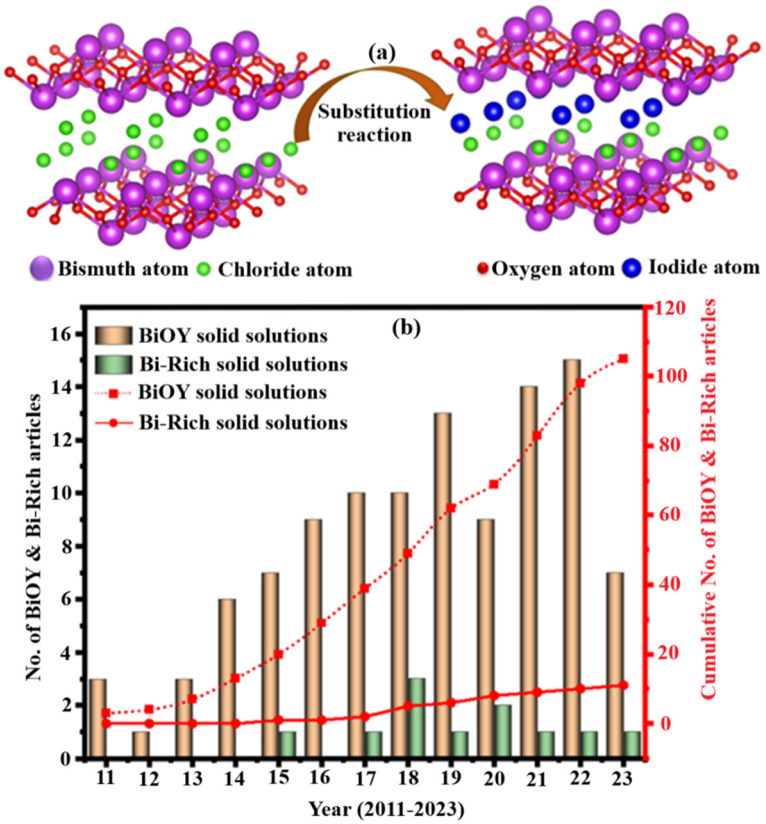

Fig. 6 a) Formation mechanism of BiOY and $Bi_xO_yY_z$ solid solutions and b) the reported number of research articles on the modification of BiOY and $Bi_xO_yY_z$ into solid solutions (Sources Web of Science, 2011–2023).

substitution of halogen atoms in a supercell with other exogenous halogen atoms. Owing to their electronic structure and atomic arrangement, halogen atoms can readily replace each other within the BiOY layered structure, allowing for a nearly arbitrary variation of halogen ions.[78] Currently, various BiOY solid solutions compositions, such as, $BiOI_xCl_{1-x}$, $BiOCl_xBr_yI_z$ $BiOCl_xBr_{1-x}$, $BiO(OH)_xI_{1-x}$, $BiO(ClBr)_{(1-x)}/2I_x$, and $BiOBr_xI_{1-x}$ have been synthesized and demonstrated to exhibit enhanced activity compared to their pure counterparts. Zhang *et al.* proposed that the heightened photocatalytic activity of BiOY solid solutions is contingent upon the modulation of band gaps. DFT computations have revealed that band gaps decrease with increasing concentrations of heavier halogen atoms, resulting in a substantial red shift of the adsorption spectra and greater utilization of sunlight.[79] The variation of EV (*vs.* NHE) with the composition, *x*, which is based on the

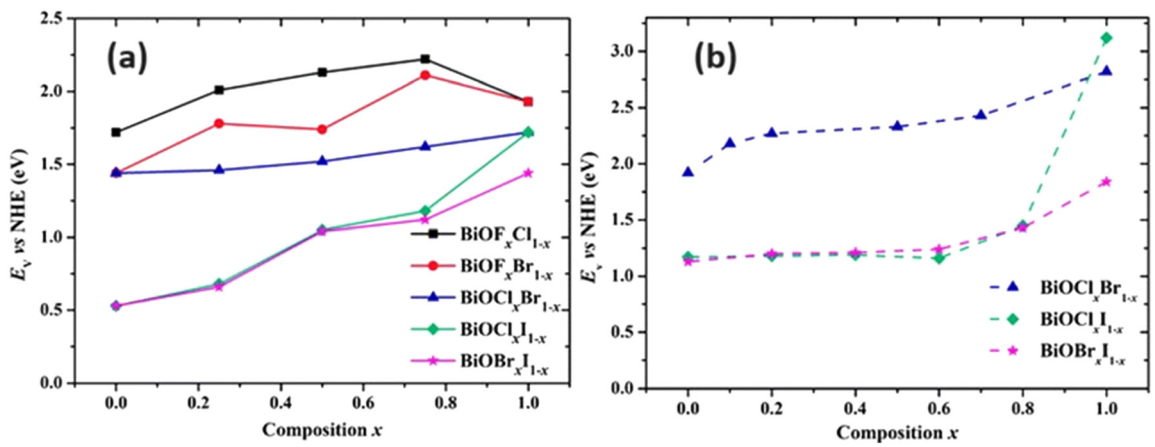

Fig. 7 Variation in E_v (*vs.* NHE) against composition of *x* for the a) computed and b) experimental band gaps of BiOY solid solutions. Reprinted with permission from ref. 79. Copyright (2012) Royal Society of Chemistry.

theoretical and experimental band gaps, is shown in Fig. 7. Furthermore, the VB constitution for BiOY comprises primary O 2p and X np orbitals,[54] leading to more positively charged VB tops with an increase in lighter halogens, indicating an enhanced oxidation potential.[79,80]

BiOY exhibits remarkable electron–hole pair separation, a crucial characteristic shared among these materials.[81] This phenomenon arises from the hybridization of X-np states, resulting in a reduced valence band maximum (VBM) and increased chemical disorder within the alloyed BiOY structure. The introduction of disorder and variation in VBM generates defect levels serve as trap centers for photogenerated holes. Consequently, this impedes the mobility of the photoexcited holes within the alloyed BiOX, thereby reducing electron–hole recombination. Wang *et al.*[82] demonstrated that $BiOBr_{0.85}I_{0.15}$, rich in oxygen vacancies (OVs), exhibited the highest photocurrent density and the smallest radius in the electrochemical impedance spectra compared to other compositions. This finding suggests a prolonged lifetime of the photoinduced charge carriers in $BiOBr_{0.85}I_{0.15}$. Essentially, the formation of a solid solution in BiOY results in a reduction of the e^-/h^+ recombination rate, consequently enhancing the photocatalytic activity. Moreover, BiOY solid solutions can easily be tailored to form OVs, which act as capture traps for photogenerated electrons, further facilitating the separation of charge carriers.

A new family of $BiO(Cl_xBr_{1-x})$ solid solutions synthesized *via* the hydrothermal method exhibited a 3 times increase in the rate of aqueous RhB removal under visible-light irradiation compared to Degussa P25. Some studies have reported the correlation between various experimental parameters and the characteristics of BiOY solid solutions. For instance, $BiOCl_{0.875}Br_{0.125}$ synthesized through a simple precipitation method at room temperature, involved the complete dissolution of $Bi(NO_3)_3{\cdot}5H_2O$ in glacial acetic acid to yield $[Bi_2O_2]^{2+}$ intermediate species. Glacial acetic acid facilitated the reaction between Bi^{3+}, halide anions, and water. Cetyltrimethylammonium chloride (CTAC) and cetyltrimethylammonium bromide (CTAB) are common structure-directing agents and halide sources.[83] Yang *et al.* conducted studies on various $BiOCl_xBr_{1-x}$ compositions to investigate the influence of the raw materials and solvents. Their findings revealed that NH_4Cl, KBr, and water favored the formation of simple stacked nanoplates, whereas polyacrylamide (C-PAM), CTAB, and glycol promoted the formation of 3D hierarchical flower-like microspheres. In principle, the formed BiOY hierarchical flower-like structure possesses a larger specific surface area and an increased number of active sites, thereby enhancing photocatalytic reactions.[84] These studies established the significant impact of fabrication methods and the inherent properties of source materials on the photocatalytic efficiency of BiOY solid solutions.

4.1.2. Bismuth-rich solid solution. The comparable atomic configurations of $Bi_xO_yX_z$, such as Bi_3O_4Br and Bi_3O_4Cl, facilitate the incorporation of various halogens into the crystal structure, substituting other halogens and forming solid solutions. This substitution leads to significant changes in the electronic structure of the resultant solid solutions, accompanied by variations in their atomic arrangements.[85] In addition to adjusting the band edge positions, variations in the electrostatic potential between the [Bi–O] and [X] layers can be induced by the non-uniform charge distribution, allowing for the modulation of the internal electric field. For instance, Sun *et al.* synthesized a range of $Bi_4O_5Br_xI_{2x}$ solid solutions using a simple homogeneous precipitation method, including $Bi_4O_5Br_2$, Bi_4O_5–$Br_{1.8}I_{0.2}$, $Bi_4O_5Br_{1.4}I_{0.6}$, Bi_4O_5BrI, $Bi_4O_5Br_{0.6}I_{1.4}$, $Bi_4O_5Br_{0.2}I_{1.8}$, and $Bi_4O_5I_2$.[86]

These solid solutions exhibited gradually adjustable band gap structures, as determined by UV-vis diffuse reflectance spectra, with $Bi_4O_5Br_{0.6}I_{1.4}$ demonstrating optimal photocatalytic activity for resorcinol degradation, which was 1.80 and 2.77 times higher than $Bi_4O_5I_2$ and $Bi_4O_5Br_2$, respectively. The enhanced photocatalytic performance of $Bi_4O_5Br_{0.6}I_{1.4}$ is attributed to the improved charge separation efficiency resulting from the formation of an internal electric field within the $Bi_4O_5Y_2$ solid solutions, which polarizes the photogenerated charges, thereby enhancing the photocatalytic activity. Substituting I with Br in $Bi_4O_5Br_{0.6}I_{1.4}$ leads to a more non-uniform charge distribution, further optimizing the charge separation and increasing the photocatalytic activity. Liquid chromatography-mass spectrometry (LC-MS) analysis identified the degradation intermediates and proposed a potential degradation pathway for resorcinol. Other solid solutions, such as $Bi_5O_7Br_{0.5}I_{0.5}$ and $Bi_{24}O_{31}Cl_xBr_{10-x}$, have also been synthesized and applied for photocatalytic pollutant removal, demonstrating the effectiveness of solid solution preparation in optimizing the photocatalytic performance.[87,88]

4.2. Influence of constructing solid solutions on the intrinsic properties of the material

The construction of solid solutions exerts a profound influence on the material's intrinsic properties, impacting factors such as the band structure, electronic properties, and charge carrier dynamics. By introducing foreign atoms into the crystal lattice, solid solutions alter the atomic arrangement and electronic configuration, leading to modifications in the band-edge positions and band-gap energies. Moreover, forming solid solutions can induce variations in the charge distribution within the material, affecting the polarization of photogenerated charges and enhancing the charge separation efficiency. These alterations in intrinsic properties play a pivotal role in dictating the photocatalytic performance of the material, making solid solution formation a promising strategy for optimizing the photocatalytic activity.[89]

4.2.1. Modulation of energy band structure. Unlike conventional doping, solid solution formation can introduce novel impurity levels, broadening the light absorption spectrum and augmenting the photocatalytic efficiency.[51] Different studies have explored the impact of different solid-solution compositions on the energy band structure of BiOY[90–96] Xie *et al.*[90] revealed that by adjusting the Cl/I ratio, there is a systematic shift in the VB position, consequently altering the bandgap and optimizing the light absorption efficiency. With

an increase in the I content, the VB position of $BiOCl_xI_{1-x}$ moves upward, reducing the band gap and widening the visible light absorption range.

Some studies have employed theoretical calculation approaches to investigate the influence of solid solution formation on energy bands. Al-Keisy *et al.*[91] examined the energy band structure of $BiOI_{0.7}F_{0.3}$ and BiOI, revealing a notable increase in the conduction band minimum (CBM) at point Z (Fig. 8a) induced by I/F solid solution formation. Zhang *et al.*[92] elucidated the role of the Cl/I solid solution in modifying the energy-band structure, highlighting the impact of the Cl/I alloy on the top of the valence band (VB) of $I_{0.25}$-BiOCl. Guo *et al.*[93] prepared different nanostructured solid solutions, including nanosheets, nanoplates, and microspheres, according to the schematic illustrated in Fig. 8b. The band structures of the three nanostructured solid solutions ($BiOBr_{0.7}Cl_{0.3}$, $BiOBr_{0.7}$-$Cl_{0.3}$, and $BiOBr_{0.7}Cl_{0.3}$) are shown in Fig. 8c. Changing the solvent, that is, using water or ethylene glycol, could effectively regulate the bandgap (E_g), conduction band energy (E_{CB}), and valence band energy (E_{VB}) of the samples.

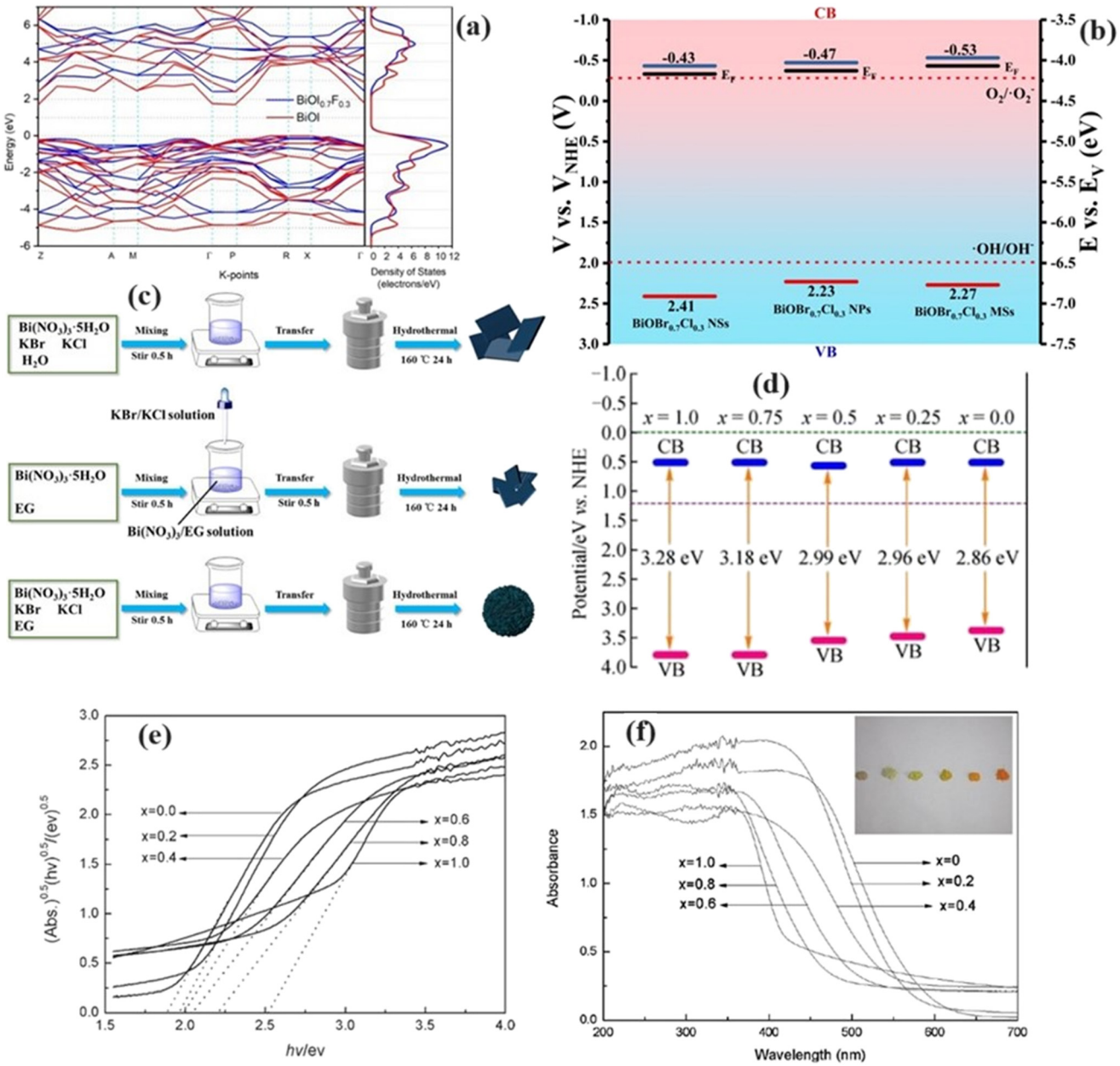

Fig. 8 a) Band structure of $BiOI_{0.7}F_{0.3}$ and BiOI according to DFT calculations. Reprinted with permission from ref. 91. Copyright (2020) John Wiley and Sons; b) band structures of nanosheets, nanoplates, and microspheres nanostructures, c) schematic illustrations of the preparation. Reprinted with permission from ref. 93. Copyright (2022) Elsevier; d) band structures of $BiOCl_xBr_{1-x}$ solid solution. Reprinted with permission from ref. 94. Copyright (2017) Springer Nature; e) band gaps, f) UV-vis diffuse reflectance spectra $BiOBr_xI_{1-x}$, with color variation shown in the inset. Reprinted with permission from ref. 95. Copyright (2017) American Chemical Society.

The experimental determination of the band gaps of solid solution-based binary halogen systems, such as $BiOCl_xBr_{1-x}$,[94] $BiOBr_xI_{1-x}$,[95] and $BiOCl_xI_y$,[96] confirms the theoretical predictions, demonstrating the effectiveness of solid solution engineering in continuously regulating the band gap. The construction of solid solutions also alters the light absorption capacity of the catalyst by modifying the band energy structure. With increasing Br content in $BiOCl_xBr_{1-x}$, the bandgap gradually decreased (Fig. 8d), enhancing the light absorption ability of the catalyst and thus improving its photocatalytic activity. Similarly, as the x value decreased in $BiOBr_xI_{1-x}$, the band gap decreased (Fig. 8e), resulting in darker coloration and enhanced absorption of visible light (Fig. 8f). These findings confirm that solid solution engineering can adjust the bandgap width, thereby expanding the range of visible light absorption, akin to the behavior observed in binary halogen solid solutions.

4.2.2. Regulation of photogenerated charge carriers. During solid-solution synthesis, structural imperfections can emerge within the crystalline lattice, acting as capture sites for photogenerated charge carriers, thereby influencing their dynamics. The disparity in mobility between different charge carriers plays a crucial role in reducing the recombination rates of photogenerated electron–hole pairs. Wang *et al.*[82] demonstrated that the formation of a solid solution in $BiOBr_xI_{1-x}$ leads to the hybridization of halogen np orbitals, which diminishes the mobility of photogenerated holes. In contrast, the migration of photogenerated electrons remains unaffected. This differential mobility between electrons and holes significantly lowers the carrier recombination rate.

The transfer pathway is crucial in determining the behavior of photogenerated charge carriers. Huang *et al.*[97] employed a novel method to reduce photogenerated carrier recombination by increasing the band gap through solid-solution formation. By incorporating bromine into BiOI, the valence band (VB) position shifts downward, lengthening the electron transfer path from the conduction band (CB) to the VB, thus hindering recombination. The variation in halogen atomic radii due to solid-solution formation alters the interlayer spacing, subsequently affecting photogenerated carriers' transfer pathways. Ren *et al.*[98] suggested that introducing fluorine, with its smaller atomic radius, into the halogen layer decreases the interlayer spacing and shortens the carrier transfer pathway. The formation of ternary solid solutions also enhances the strength of the built-in electric field, promoting the separation and transfer of charge carriers.

Other studies have demonstrated the significant influence of solid solution formation in modulating the carrier behavior. Solid solution engineering facilitates the spatial segregation of carriers through bandgap expansion, establishment of electron capture traps, and alteration of photogenerated hole mobility, thereby effectively suppressing carrier recombination. This phenomenon is advantageous for enhancing the photocatalytic performance of the catalysts.[89] Further, the intrinsic properties of solid solutions can be improved through various techniques. These include morphological control, optimization of optical properties, and facet modification. Additionally, controlling oxygen vacancies (crystal vacancy defects) and synergizing with other modification techniques, such as cation doping, establishing heterojunctions, and inducing plasma resonance effects. These methods are described as follows:

4.2.3. Morphological control. Solid solution materials of BiOY and $Bi_xO_yY_z$ are crucial for photocatalysis, particularly for the utilization of visible light. However, the photocatalytic performance of BiOY and $Bi_xO_yY_z$ solid solutions can still be further improved. Nanoscale morphological engineering through a synthesis process has been conducted to endow solid solutions with unique characteristics for enhanced performance.[99] This section provides an overview of the morphological control of BiOY and $Bi_xO_yY_z$ solid-solution materials employed as photocatalysts in recent studies. This summary encompasses one-dimensional (1D) nanorods, nanowires; two-dimensional (2D) nanosheets, nanoplates; three-dimensional (3D) nanospheres, and the creation of hierarchical and hollow structures. A schematic representation of light undergoing multiple reflections within various structures is illustrated in Fig. 9, including nanospheres formed by the assembly of nanosheets and nanoparticles, isolated nanosheets, hollow nanospheres with interior and exterior views, and nanorods.[6]

4.2.3.1. One-dimensional morphology. One-dimensional nanostructures, including nanorods, nanowires, nanofibers, and nanotubes, are characterized by a high length-to-diameter ratio and offer notable benefits. These advantages include substantial surface area, distinct longitudinal movement pathways for charge carriers, extensive exposure to active sites, and improved light absorption and scattering properties. Zhang *et al.* (2020) demonstrated that 1D $Bi_{12}O_{17}Cl_xBr_{2-x}$ ($Bi_{12}O_{17}ClBr$) nanotube solid solution with rich oxygen vacancies could achieve 93% tetrachlorobiphenyl A (TCBPA) degradation. The tubular structure of the nanotubes, shown in Fig. 10, allows for efficient light absorption and redox capabilities, enhancing their photocatalytic activity. Additionally, the presence of oxygen

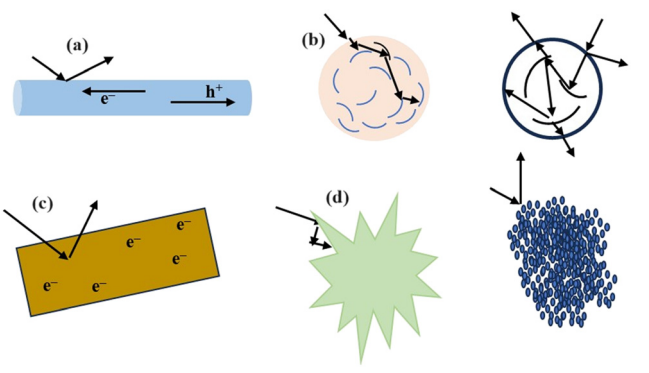

Fig. 9 A schematic illustration depicting multiple reflections within different structures: a) nanorod, b) nanosheets, c) hollow nanoparticles, and d) nanospheres assembled by nanosheets.

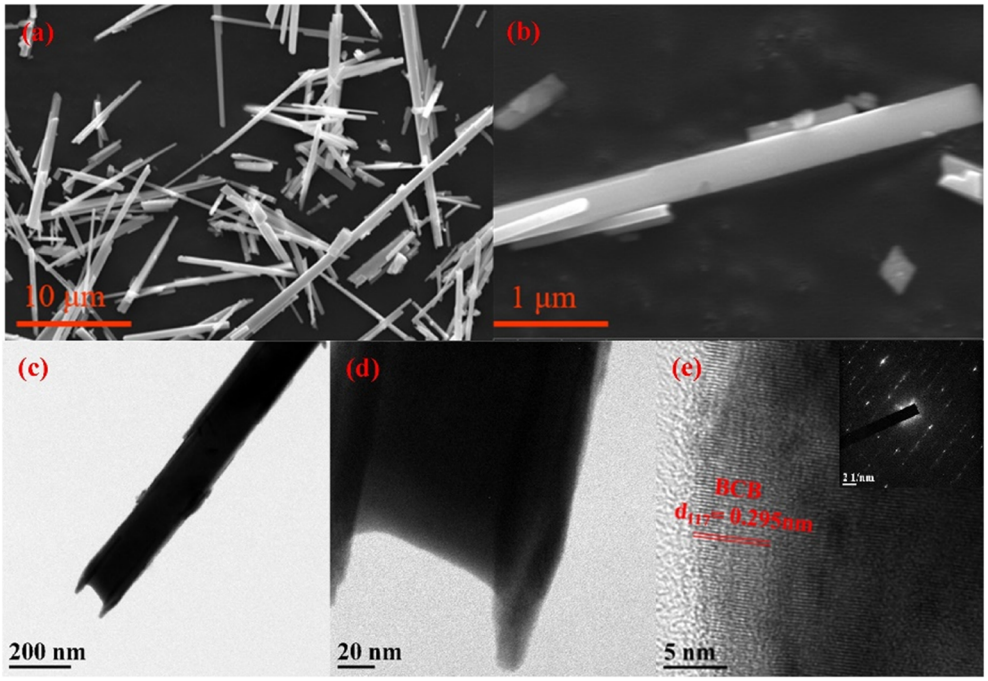

Fig. 10 a and b) SEM, c and d) TEM, and e) high-resolution TEM images of 1D $Bi_{12}O_{17}ClBr$ nanotubes. Reprinted with permission from ref. 100. Copyright (2020) Elsevier.

vacancies in nanotubes contributes to the generation of superoxide and hydroxyl radicals, which play essential roles in the photocatalytic degradation of the target pollutant.[100]

4.2.3.2. Two-dimensional morphology. There has recently been increasing attention toward low-dimensional materials, mainly 2D nanosheets, and nanoplates, for energy conversion and environmental remediation.[101] 2D nanostructures offer expanded surface areas, providing ample reactive sites for redox reactions, with manageable adjustments in the exposed facets.[102,103] Thi *et al.*[104] synthesized high-quality BiOBr, BiOCl, and $BiOCl_{1-x}Br_x$ solid solutions in nanoplate form (Fig. 11a), with $BiOCl_{0.5}Br_{0.5}$ solid solutions showing unique morphologies because of the increased Cl^- content. The preparation of Bi_5O_7I/$BiOBr_xI_{1-x}$ heterostructures *via* hydrobromic acid etching yielded rod-like morphologies (Fig. 11b), which were controlled by pH variations.[105] Additionally, solvothermal methods produce $BiOCl_{0.5}Br_{0.5}$ solid solution nanosheets and $BiOCl_{1-x}Br_x$@AgBr heterostructures (Fig. 11c), enhancing photocatalytic activity by increasing the surface area and charge separation.[106,107] Varying the Br/I ratio resulted in ultrathin $BiOBr_xI_{1-x}$ 2D nanosheets with enhanced degradation abilities, indicating the potential for improved pollutant removal.[108,109] Furthermore, $BiOCl_{0.5}Br_{0.5}$ nanoplates (Fig. 11f) with exposed {001} facets display enhanced photocatalytic performance, suggesting their suitability for environmental applications.[110] Morphological studies of the $BiOCl_{0.25}Br_{0.75}$ and Au-$BiOCl_{0.25}Br_{0.75}$ (Fig. 11g) composites revealed intact heterojunctions, indicating potential enhancements in the degradation efficiency through effective charge transfer mechanisms.[111] These observations underscore the significance of morphological characteristics in enhancing the efficiency of bismuth-based photocatalysts.

4.2.3.3. 3D morphology. Increasingly, there is a growing recognition of the role hierarchical nanostructures play in enhancing the photocatalytic performances of BiOY and $Bi_xO_yY_z$ solid solutions. These structures, typically composed of nanosheets, offer increased specific surface areas and multiple light reflections, enhancing photon absorption. Different synthetic techniques have been explored to control the morphology of these materials.[112–114] For example, $BiOCl_{1-x}Br_x$ samples prepared *via* precipitation at ambient temperature exhibit uniform flower-like architectures (Fig. 12a) with porous structures.[115] Whereas chemically synthesized C-$BiOBr_{0.5}I_{0.5}$ composites display irregular nanoplates, leaf-extract-mediated G-$BiOBr_xI_{1-x}$ composites form 3D hierarchical nanospheres (Fig. 12b).[116] Additionally, the morphologies of the $BiOCl_xI_y$ solid solutions varied with the Cl-to-I molar ratio, influencing the formation of flower-like microspheres or clustered nanoplates (Fig. 12c).[115,116] Incorporating additives such as $BiPO_4$ did not alter the hierarchical microflower morphology of $BiOCl_{0.75}Br_{0.25}$, indicating successful heterostructure formation.[117] Furthermore, the addition of KI during synthesis influenced the morphology of the $BiOCl_xBr_yI_z$ samples, with varying ratios resulting in different structures, from interleaved wafer-like particles to more extensive and more compact hierarchical spheres (Fig. 12d).[118,119]

4.2.4. Crystal vacancy defect. Oxygen vacancies (OVs) serve as pivotal defects in semiconductor photocatalysts, such as BiOCl, profoundly influencing their photocatalytic performance by expanding light absorption and enhancing photoreactivity. The formation of OVs is particularly notable in ultrathin structures such as nanosheets, which expose a more significant number of surface atoms, facilitating vacancy creation.[6,54,121]

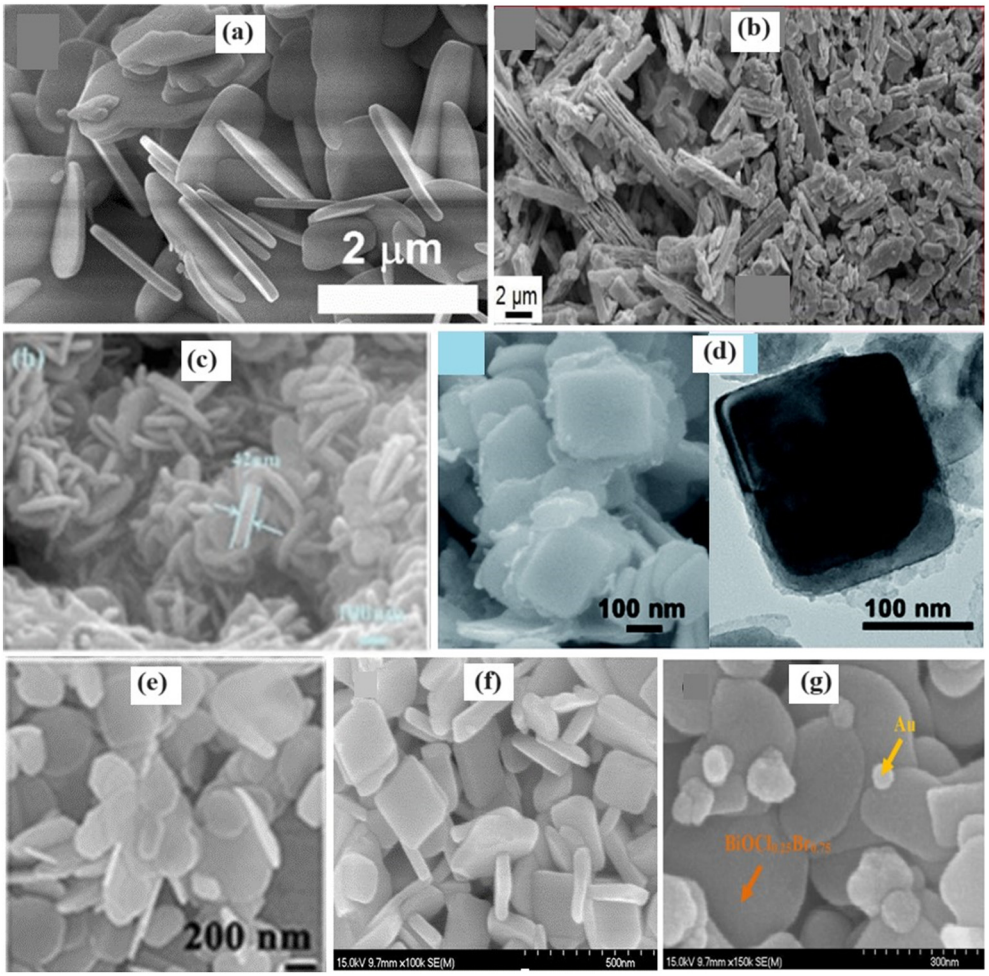

Fig. 11 FESEM of a) $BiOCl_{0.5}Br_{0.5}$ nanoplate. Reprinted with permission from ref. 104. Copyright (2023) Elsevier; b) $Bi_5O_7I/BiOBr_xI_{1-x}$ heterostructures. Reprinted with permission from ref. 105. Copyright (2023) Elsevier; c) 3CQDs–$BiOCl_{0.5}Br_{0.5}$ nanosheet structures. Reprinted with permission from ref. 106. Copyright 2022 American Chemical Society; d) $BiOCl_{1-x}Br_x$@AgBr heterostructures;[107] e) 2D $BiOCl_{0.5}Br_{0.5}$ nanoplates. Reprinted with permission from ref. 110. Copyright (2015) John Wiley and Sons; f) $BiOCl_{0.25}Br_{0.75}$ and g) 1.3% Au-$BiOCl_{0.25}Br_{0.75}$ composite. Reprinted with permission from ref. 111. Copyright (2017) Elsevier.

Alansi *et al.*[122] demonstrated the remarkable photochromic response of 3D-$BiOCl_{0.8}Br_{0.2}$ nanoflowers, transitioning from white to black under sunlight owing to OV formation (Fig. 13a–c). Zhang *et al.*[123] showed the controllable introduction of OVs by adjusting the halogen composition in BiOY solid solutions, highlighting the significantly higher OV concentration in Br-solid solution-based BiOY compared to pure BiOY. Additionally, the prepared $BiOCl_xI_{1-x}$ solid solution with variable Cl to I ratios exhibited OV formation.[124] Ji *et al.*[125] revealed the significant impact of the OV content on the carrier recombination rates in a $BiOCl_{0.5}I_{0.5}$ solid solution, where a higher OV content led to enhanced carrier migration and reduced recombination rates (Fig. 13d). Ren *et al.*[98] synthesized F/Br/I ternary halogen solid solution-based BiOY with varying OV contents and observed that a higher OV content effectively suppressed photogenerated carrier complexes, thereby improving the carrier lifetime.

Xu *et al.*[126] also employed a molten salt approach to produce $BiOCl_{1-3x}I_{3x}$ with an increased OV concentration compared to traditional hydrothermal methods. They underscored the critical role of OVs in enhancing photocatalytic performance and offered insights into strategies for controlling the OV content in semiconductor photocatalysts. Other studies reported that the improved carrier separation efficiency was attributed to introducing OVs into the solid solution. These vacancies, formed by the absence of oxygen atoms, act as traps for capturing photoexcited electrons, impeding carrier recombination and promoting the adsorption and activation of small molecules during interfacial reactions, thereby enhancing the reaction efficiency.[79,127] Moreover, Guo *et al.* reported that the presence of various oxygen species, including lattice oxygen (OL), weakly bound or chemisorbed oxygen (OC), and OV/OT (OT = OV + OL + OC), provides insights into the relationship between the OV concentration and solid solution ratio.[128]

4.2.5. Other integrated intrinsic properties enhancement strategies. The synergistic augmentation effect achieved through the integration of diverse modification techniques is widely recognized for its positive impact on the photocatalytic efficacy of the catalyst. Incorporating solid solutions with

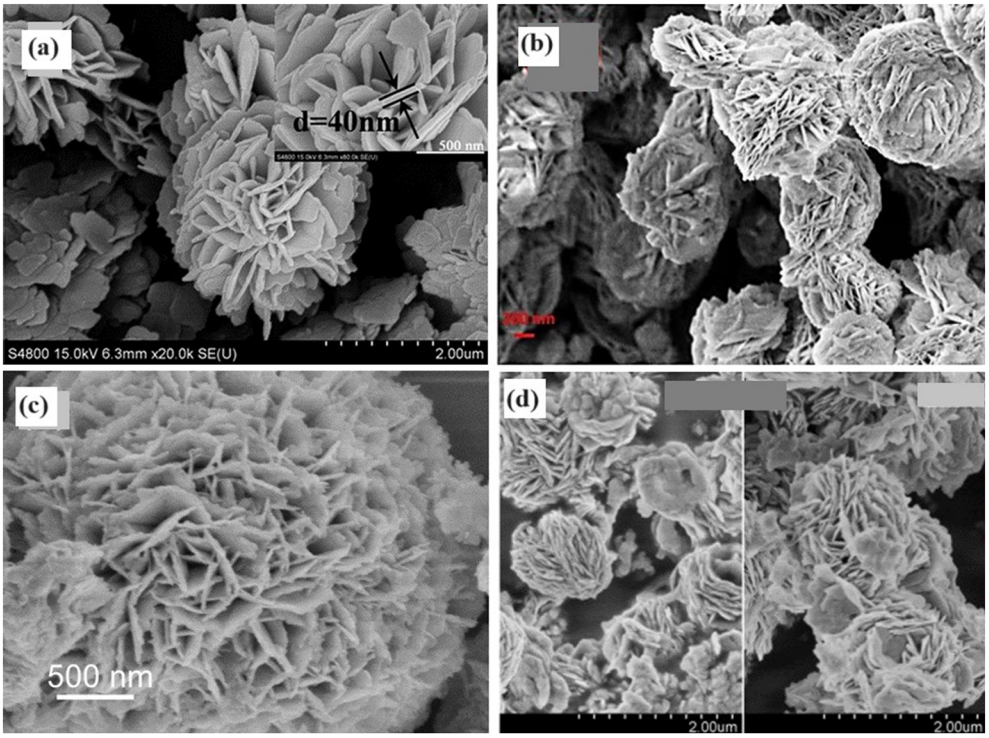

Fig. 12 The morphologies of the 3D structures of a) $BiOCl_{1-x}Br_x$. Reprinted with permission from ref. 115. Copyright (2016) Elsevier; b) G-$BiOBr_xI_{1-x}$ composites. Reprinted with permission from ref. 116. Copyright (2019) Elsevier; c) $BiOCl_3I$. Reprinted with permission from ref. 120. Copyright (2016) Elsevier; and d) $BiOCl_xBr_yI_z$. Reprinted with permission from ref. 117. Copyright (2015) Elsevier.

additional modification approaches significantly expands the scope of design possibilities and potential applications of BiOY and $Bi_xO_yY_z$ materials. Researchers have merged solid solutions with an array of modification techniques to refine the intrinsic characteristics and improve the photocatalytic performance of BiOY and $Bi_xO_yY_z$ materials.

4.2.5.1. Solid solution combined with metal or nonmetal. Metal doping has long been a viable method for fine-tuning BiOY and $Bi_xO_yY_z$ band structures, enhancing the carrier separation efficacy. Theoretical modeling has demonstrated that the combined impact of metal doping and solid solution reduces the catalyst's band gap and improves its oxidative capabilities, offering significant advantages in the photooxidation of contaminants.[129] Qi *et al.*[111] documented that incorporating Au into $BiOCl_{1-x}Br_x$ enhanced the photocatalytic activity of the composite materials. The interplay between Au NPs and $BiOCl_{1-x}Br_x$ led to elevated Schottky barriers. Au NPs acted as electron reservoirs, fostering the disjunction of e^-/h^+ pairs and advancing interfacial electron transfer. Furthermore, these nanoparticles demonstrate robust absorption of visible light owing to surface plasmon resonance, augmenting optical absorption and photocatalytic efficacy when exposed to visible light irradiation.[130]

Similarly, Han *et al.*[131] engineered Fe^{3+}-doped $BiOCl_xI_{1-x}$ (Fe–$BiOCl_xI_{1-x}$@AP) supported on amidoxime-functionalized fibers. The Fe–O–Bi coordination site enhanced Fe–$BiOCl_xI_{1-x}$ light absorption *via* electron transfer. The fiber support, Fe ions, and Cl/I alloy synergistically promoted electron transfer. This mechanism involved the transfer of electrons from O^{2-} to the Bi^{3+} 6p orbital in $BiOCl_xI_{1-x}$, with the addition of Fe^{3+} enhancing this transfer through electron repulsion interactions. Moreover, the amidoxime moieties on the fiber substrate contributed lone pair electrons to Fe^{3+}, thereby promoting electron transfer from O^{2-} to Bi^{3+}. Consequently, Fe–$BiOCl_xI_{1-x}$@AP exhibited a superior tetracycline photodegradation performance.

4.2.5.2. Solid solutions with heterojunction. Solid solution construction narrows the energy band gap, intensifies light absorption, and increases carrier recombination. Conversely, the electric fields of heterojunctions segregate carriers, mitigating the drawbacks of solid solutions. The stratified BiOY and $Bi_xO_yY_z$ solid solutions enhanced the interfacial contact, improving charge transfer during heterojunction formation. Combining solid solutions and heterostructures reduced the bandgap, enhanced light absorption, and stabilized the photocatalytic systems by mitigating carrier recombination through heterojunction electric fields.[132]

The heterojunction between $BiOBr_{0.75}I_{0.25}$ and $BiOIO_3$ was prepared *via* a simple deposition–precipitation technique, which showed the distinct features of $BiOBr_{0.75}I_{0.25}$ and $BiOIO_3$. $BiOBr_{0.75}I_{0.25}$ has a narrow energy band gap (2.02 eV) responsive to visible light, whereas $BiOIO_3$ has a wider band gap (2.87 eV) and is less responsive to visible light. Heterojunction formation allows for an advantageous combination of these materials, improving the photocatalytic performance of the composite. The interface between

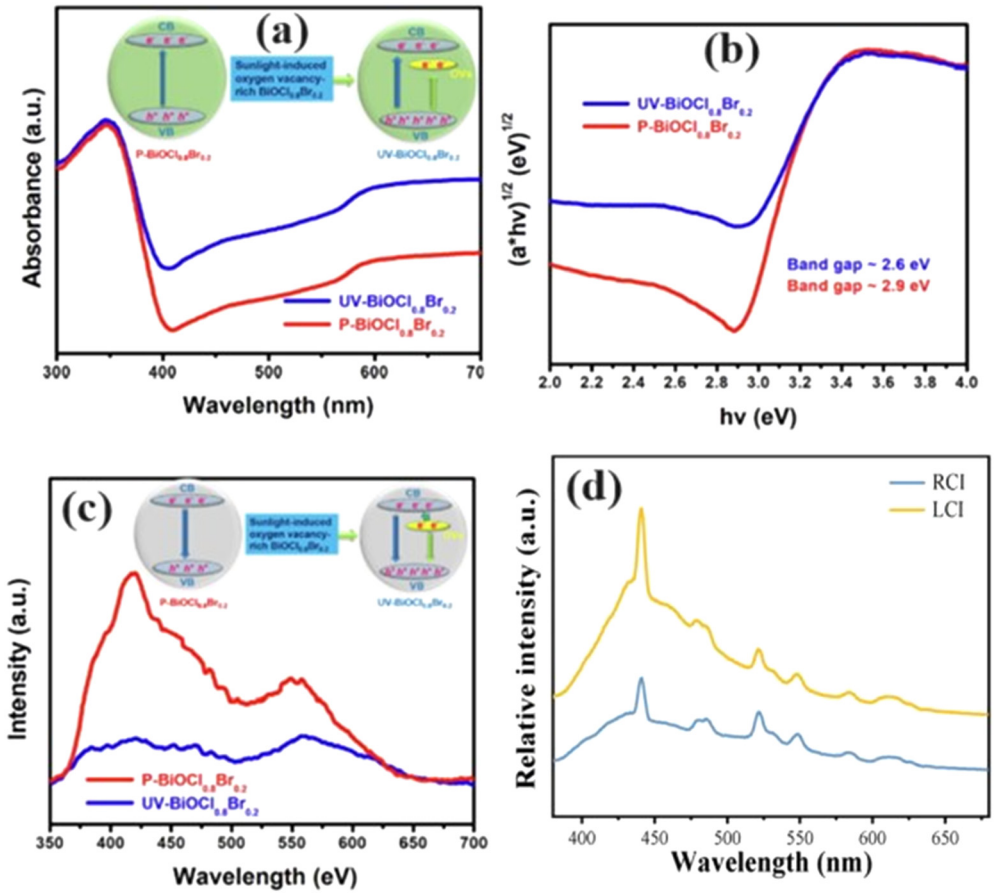

Fig. 13 a) UV-vis diffuse reflectance spectra, b) band gap energies from Tauc plots, c) photoluminescence emission spectra of the P-$BiOCl_{0.8}Br_{0.2}$ and UV- $BiOCl_{0.8}Br_{0.2}$. Reprinted with permission from ref. 122. Copyright (2022) Elsevier; d) PL spectra of $BiOCl_{0.5}I_{0.5}$ rich in OV (RCI) and $BiOCl_{0.5}I_{0.5}$ less rich in OV (LCI). Reprinted with permission from ref. 125. Copyright (2022) Elsevier.

$BiOBr_{0.75}I_{0.25}$ and $BiOIO_3$ facilitated the separation and transfer of photoexcited charge carriers, significantly promoting the degradation of pollutants under visible light irradiation.[133]

The formation of BiOY/Ag_3PO_4, BiOY/Fe_3O_4@SiO_2, and BiOY/TiO_2 heterostructures can facilitate efficient electron transfer and separation of charge carriers, resulting in improved photocatalytic activity under visible-light irradiation. These heterostructures exhibited improved degradation of phenol, PPCPs, benzophenone-3, ibuprofen, and RhB dye compared with BiOY solid solution. These heterojunctions exploit the unique properties of each material to broaden the range of light absorption (Fig. 14a) and enhance the overall efficiency of photocatalysis.[131–133] Another strategy involves exploring 2D–2D interface heterojunctions (Fig. 14b), such as Ag_3PO_4-$BiOCl_{1-x}Br_x$,[65] $BiOCl_xBr_{1-x}$/GO[66] and Ti_3C_2/$BiOCl_xBr_{1-x}$,[134] which provided enhanced gas adsorption and electron–hole pair separation capabilities. These structures promote synergistic effects between the components, resulting in an enhanced photocatalytic activity for the degradation of various pollutants.

Moreover, several studies have emphasized the significance of heterojunction interfaces in promoting efficient charge transfer and separation. Heterojunctions with well-developed interfaces, such as Bi_5O_7I/$BiOBr_xI_{1-x}$[67] or $BiOCl_{1-x}Br_x$@AgBr,[107] exhibit superior photocatalytic performance owing to the enhanced separation of electron–hole pairs and extended carrier lifetime (Fig. 14c). The reported study introduces a direct redox-mediator-free Z-scheme heterojunction between $BiPO_4$ and $BiOCl_{0.9}I_{0.1}$, prepared through a water bath reaction at 90 °C. This synthesis method ensured a close interfacial contact between the two materials, forming a heterostructure with multiple vacancies and valences. These defects, including Bi^{5+}, Bi^{3+}, $Bi^{(3-x)+}$, I^-, I^{3-}, and IO_3^-, promoted efficient charge separation and transfer during photocatalysis (Fig. 14d).[136]

4.2.5.3. Solid solutions with carbon-based compounds. Further improvement of the intrinsic properties of BiOY and $Bi_xO_yY_z$ was achieved by investigating the influence of carbon-based compounds such as graphitic carbon nitride (g-C_3N_4), graphene, and carbon quantum dots (CQD) in improving the photocatalytic capacity of BiOY and $Bi_xO_yY_z$ solid solutions.[89] These carbon-based compounds have been explored due to their synergistic properties and high surface areas.[137] g-C_3N_4 emerged as a promising material despite its limited carrier separation efficiency. Combining g-C_3N_4 with BiOY and $Bi_xO_yY_z$ led to heterostructures with enhanced photocatalytic efficacies.[89]

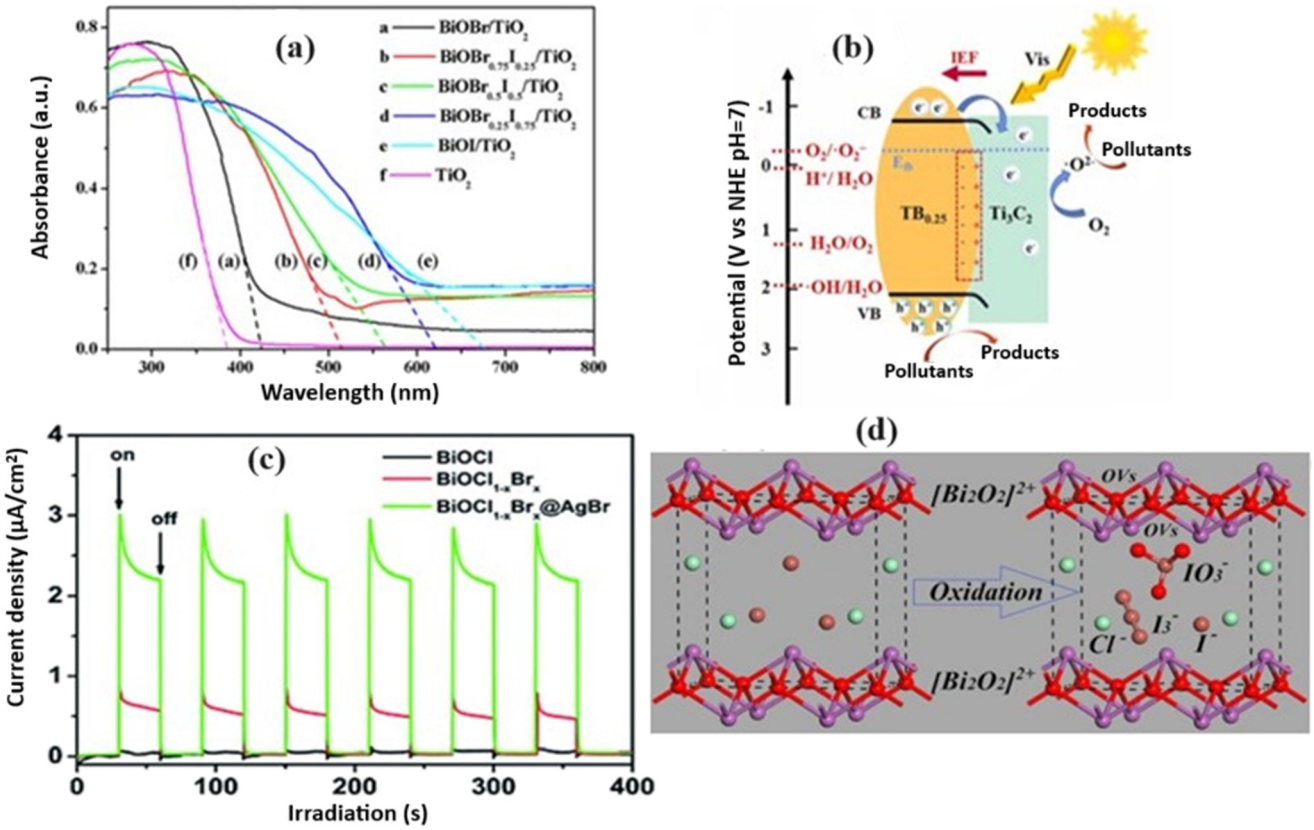

Fig. 14 a) UV-vis diffuse reflectance spectra of TiO_2–$BiOBr_xI_{1-x}$ heterojunctions and TiO_2 NRs. Reprinted with permission from ref. 135. Copyright (2020) Elsevier; b) 2D/2D interfaces of Ti_3C_2/$BiOCl_xBr_{1-x}$. Reprinted with permission from ref. 134. Copyright (2023) Elsevier; c) transient photocurrent responses of BiOCl, $BiOCl_{1-x}Br_x$, *and* $BiOCl_{1-x}Br_x$@AgBr. Reprinted with permission from ref. 107. Copyright (2023) Elsevier; d) schematic representation illustrating the mechanism of IO_3^- and I_3^- ions formation for $BiOCl_{0.9}I_{0.1}$. Reprinted with permission from ref. 136. Copyright (2019) Elsevier.

A type II g-C_3N_4/$BiOCl_{0.2}Br_{0.8}$ heterojunction was fabricated using a straightforward immersion-precipitation technique.[138] Remarkably, g-C_3N_4/$BiOCl_{0.2}Br_{0.8}$ exhibited an extended photoluminescence lifetime compared to pristine g-C_3N_4, indicating enhanced carrier separation efficiency. This augmentation enhanced RhB degradation activity for g-C_3N_4/$BiOCl_{0.2}Br_{0.8}$ compared to the individual g-C_3N_4 and $BiOCl_xBr_{1-x}$ counterparts.[138] To augment the efficacy of organic pollutant elimination, a type-II g-C_3N_4/$BiOCl_xI_{1-x}$ heterojunction (BCI-CN-P) rich in OV was synthesized *via* a precipitation technique aided by PVP.[139] The mechanism of carrier transfer (Fig. 15a) revealed preferential photogenerated electron migration towards OV-induced defect sites before transitioning to the CB at a lower energy level. The photocurrent characteristics (Fig. 15b) highlighted the synergistic effect of the solid solution, heterojunction formation, and OV in inhibiting photogenerated electron–hole recombination. Consequently, BCI-CN-P demonstrated remarkable efficiency in complete BPA degradation within 40 min.[139] To enhance the semiconductor's redox potential and enhance the efficiency of RhB degradation, a Z-scheme graphene-like g-C_3N_4)/$BiOCl_xI_{1-x}$ heterojunction was fabricated through *in situ* deposition. A systematic investigation was conducted to determine the optimal composition of the catalyst for RhB degradation, and the photoelectric properties of the catalysts were evaluated. Notably, the 10-CN/$BiOCl_{0.8}I_{0.2}$ composite showed reduced photoluminescence intensity, increased photocurrent, and lowered resistance, indicating the practical separation of charge carriers by the catalyst.[140]

The preparation of g-C_3N_4-$BiOCl_xBr_{1-x}$ hybrids *via* a solvothermal method was aimed at exploring the synergistic effects of combining these materials in a direct Z-scheme heterojunction. The resulting heterojunction exhibited improved photocatalytic performance, attributed to effective charge separation, surpassing that of pristine g-C_3N_4 and $BiOCl_{0.5}Br_{0.5}$.[144] Engineered band structure improvements bolstered the light absorption, redox capabilities, and transfer of charge carriers. The direct Z-scheme mechanism retains a strong redox potential, further enhancing the photocatalytic performance.[144] A 3D hybrid photocatalyst integrating g-C_3N_4 and $BiOBr_{0.2}I_{0.8}$ *via* hydrothermal synthesis showed a tailored band structure.[141] Tailoring the energy-band alignments facilitates efficient charge migration at the heterojunction interface. The formed heterojunction significantly enhanced the charge separation, providing a conducive environment for separating electron–hole pairs and improving the quantum efficiency. X-ray photoelectron spectroscopy analysis (Fig. 15c) revealed a distinct channel for photogenerated charge transmission within the heterojunction. Compared with bare g-

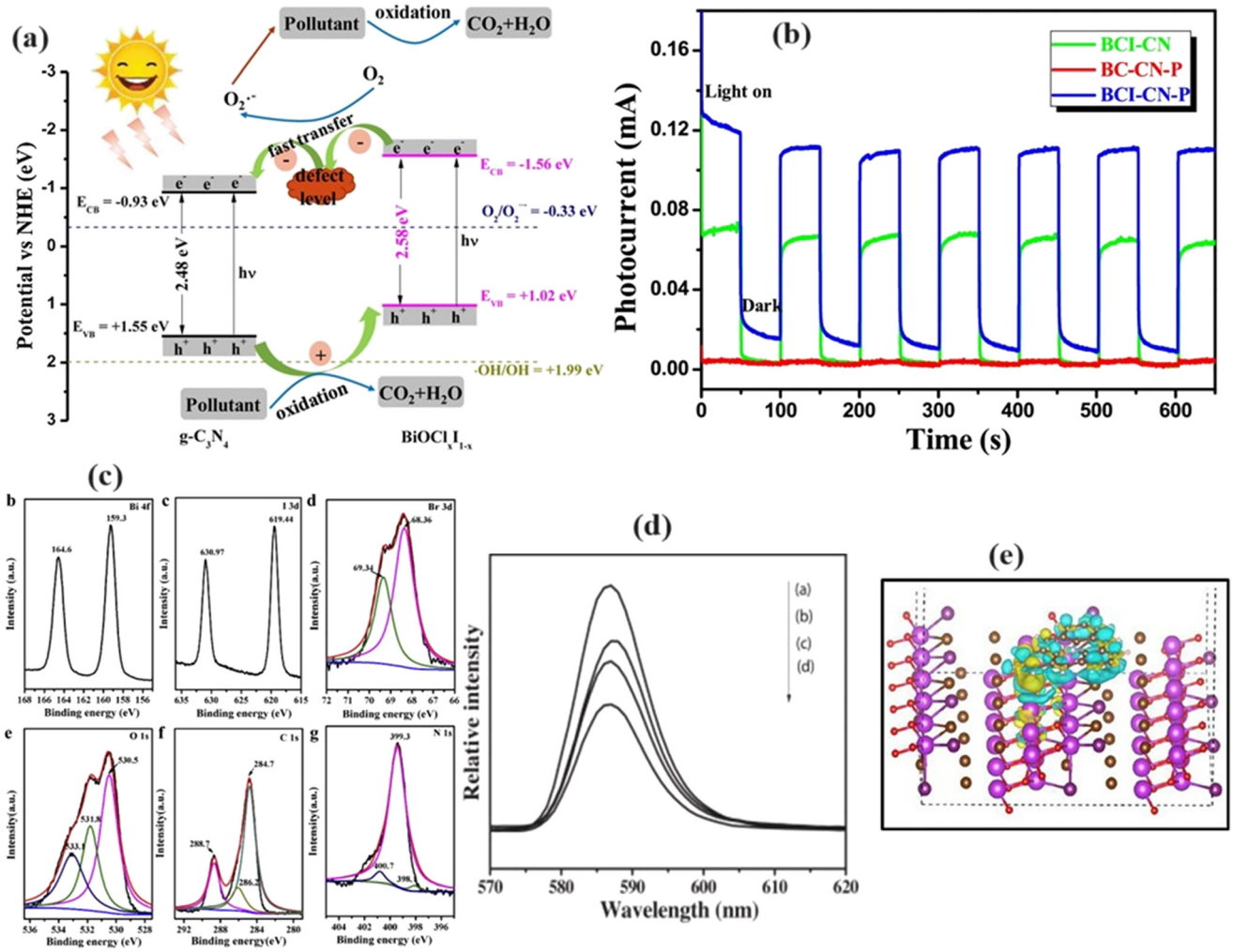

Fig. 15 a) Energy band structures and electron–hole pairs separation over BCI-CN-P nanosheets, b) transient photocurrent responses. Reprinted with permission from ref. 139. Copyright (2019) Elsevier; c) X-ray photoelectron spectroscopy of g-C_3N_4 and $BiOBr_{0.2}I_{0.8}$. Reprinted with permission from ref. 141. Copyright (2018) Elsevier; d) PL spectra of the as-synthesized samples. Reprinted with permission from ref. 142. Copyright (2013) Elsevier; e) 3D charge density differences of N-CQD/$BiOI_{0.25}Br_{0.75}$: yellow and blue isosurfaces indicate charge accumulation and depletion, respectively, compared to isolated N-CQD and $BiOI_{0.25}Br_{0.75}$. Reprinted with permission from ref. 143. Copyright (2020) Elsevier.

C_3N_4 and $BiOBr_{0.2}I_{0.8}$, the 3D hybrid photocatalyst demonstrated a notable improved photocatalytic performance, primarily ascribed to effective separation of charge carriers.[141]

Using a solvothermal technique, graphene sheets were grafted onto three-dimensional microspheres of $BiOBr_{0.2}I_{0.8}$, comprising nanoplates uniformly dispersed across the graphene surface. This amalgamation facilitated augmented separation and transfer of charges, as confirmed by photoluminescence findings (Fig. 15d). The composite showed diminished electron–hole recombination rates, credited to electron migration from the VB to the CB and subsequently to the graphene sheets, thereby impeding direct recombination.[142] The composite of $BiOBr_{0.2}I_{0.8}$/graphene exhibited remarkable photocatalytic efficacy in the degradation of rhodamine B (RhB) and phenol under visible-light illumination.[142] N-doped CQDs (N-CQDs) were incorporated into a $BiOI_xBr_{1-x}$ solid solution forming N-CQDs/$BiO_{I0.25}Br_{0.75}$ heterojunction through *in situ* co-precipitation. The binding affinity between $BiOI_xBr_{1-x}$ and N-CQDs was facilitated by the interaction of amino and carboxyl groups on N-CQDs' surface with Bi atoms in the precursor compounds derived from bismuth. This interaction led to enhanced charge transfer (Fig. 15e) and improved the intrinsic properties of the photocatalyst. The hierarchically layered microspheres of $BiOI_xBr_{1-x}$, composed of nanosheets, facilitated multiple reflections of light, thereby enhancing light harvesting. The combined effect of light scattering and the internal electric field from N-CQDs to $BiOI_{0.25}Br_{0.75}$ contributed to enhanced photocatalytic activity.[143]

4.3. Decomposition of pollutants in water and in air

Different water contaminants such as organic dyes,[145,146] metal ions,[147,148] phenolic compounds,[149,150] *p*-hydroxyphenylacetic acid,[151] pharmaceuticals,[146] and personal care products[152] have been widely reported to have negative impacts on the global ecosystem and human health. The oxidative-reductive

interactions between BiOY, $Bi_xO_yY_z$ and aquatic pollutants rely on the reactive species generated by electrons or holes. It is feasible to fabricate BiOY and $Bi_xO_yY_z$ materials with tailored light absorption capabilities through deliberate control of the structural configuration during synthesis. This enables customization of the photocatalytic characteristics to suit specific applications in this domain.[19]

4.3.1. Removal of dyes. Inspired by the discovery of the photocatalytic efficacy of BiOY and $Bi_xO_yY_z$ photocatalysts, a range of engineered BiOY and $Bi_xO_yY_z$ materials with layered structures, has been employed for the degradation of different organic dyes, including RhB,[85,145] MO,[84] MB,[4] Reactive Blue KN-R,[107] MG,[153] and acid orange 7.[154] Table 1 shows the literature on the photocatalytic degradation of different dyes over BiOY and $Bi_xO_yY_z$ solid solutions. Some researchers have reported that solid solutions of BiOY and $Bi_xO_yY_z$, in comparison to their pure forms, demonstrated a remarkable capability to achieve complete removal of RhB, MO, and MG dyes, thereby underscoring their enhanced efficiency in dye-removal processes.[84,87,153–156]

Solid solutions such as $BiOBr_{0.5}I_{0.5}$,[153] $BiOBr_{0.25}I_{0.75}$,[155] and $BiOCl_{0.75}I_{0.25}$ (ref. 156) exhibit complete degradation of dyes under visible light, attributed to their oxidation ability, valence band potential, and high specific surface area. Additionally, $BiOCl_{1-x}Br_x$ solid solutions, particularly at x = 0.5, showed enhanced activity in dye degradation owing to efficient electron–

Table 1 Summary of the reported literature on the photocatalytic degradation of various organic dyes using BiOY and $Bi_xO_yY_z$ solid solution

Solid solution material	Synthesis method	Contaminant & dosage	Irradiation source	Photocatalytic activity & active species	Ref.
$BiOCl_{1-x}Br_x$; $BiOCl_{0.5}Br_{0.5}$	Hydrothermal $Bi(NO_3)_3{\cdot}5H_2O$, water	20 mg L^{-1} RhB, 1 g L^{-1}	Visible light	97% in 60 min higher than BiOCl (48%) & BiOBr (45%)	80
$BiOCl_xBr_{1-x}$; $BiOCl_{0.5}Br_{0.5}$	Glycol-assisted hydrothermal $Bi(NO_3)_3{\cdot}5H_2O$, polyacrylamide & cetyltrimethylammonium bromide	20 mg L^{-1} MO, 1 g L^{-1}	Visible light	98.27% in 60 min ~10.9, 2.7, & 29.8 times higher than pure BiOCl, BiOBr & TiO_2, respectively. $^{\cdot}O_2^-$, h^+, & $^{\cdot}OH$	84
$Bi_4O_5Br_xI_{2-x}$; Bi_4O_5BrI,	Solvothermal $Bi(NO_3)_3{\cdot}5H_2O$, polyethylene glycol	10 mg L^{-1} RhB, 0.1 g L^{-1}	Simulated solar light	99% in 30 min h^+, $^{\cdot}O_2^-$, & e^-	85
$Bi_{24}O_{31}Cl_xBr_{10-x}$; $Bi_{24}O_{31}Cl_5Br_5$	Solvothermal $Bi(NO_3)_3{\cdot}5H_2O$, ethylene glycol	15 mg L^{-1} RhB, 0.5 g L^{-1}	Visible light	98.9% in 30 min ~1.6 & 1.9 times higher than $Bi_{24}O_{31}Br_{10}$ & $Bi_{24}O_{31}Cl_{10}$, respectively. $^{\cdot}O_2^-$ & h^+	88
$BiOCl_{1-x}Br_x$ ($0 \le x \le 1$); $BiOCl_{0.6}Br_{0.4}$	Etching process Bismuth glass, H_2SO_4	10 wt% RhB	Visible light	93.6% in 40 min	145
$BiOBr_xI_{1-x}$; $BiOBr_{0.5}I_{0.5}$	Precipitation $Bi(NO_3)_3{\cdot}5H_2O$, ethylene glycol	20 mg L^{-1} MG, 0.4 g L^{-1}	Visible light	~100% in 120 min h^+	153
CFC/$BiOBr_xI_{1-x}$; CFC/$BiOBr_{0.8}I_{0.2}$	Solvothermal $Bi(NO_3)_3{\cdot}5H_2O$, DMF, ethylene glycol	20 mg L^{-1} acid orange 7	Visible light	94.1% in 120 min	154
$BiOBr_xI_{1-x}$ (x = 0.0–1.0); $BiOBr_{0.25}I_{0.75}$	Solvothermal $Bi(NO_3)_3{\cdot}5H_2O$, ethylene glycol	10 mg L^{-1} RhB, 0.2 g L^{-1}	Visible light	100% in 20 min $^{\cdot}O_2^-$	155
$BiOCl_xI_{1-x}$; $BiOCl_{0.75}I_{0.25}$	Alcoholysis $Bi(NO_3)_3{\cdot}5H_2O$, ethyl alcohol	20 mg L^{-1} RhB, 1 g L^{-1}	Visible light	~100% in 150 min BiOCl (81.2%) and BiOI (31.5%) in 240 min	156
$BiOBr_xI_{1-x}$; $BiOBr_{0.75}I_{0.25}$	Ultrasonication synthesis. $Bi(NO_3)_3{\cdot}5H_2O$, acetic acid	20 mg L^{-1} RhB, 1 g L^{-1}	Visible light	h^+	157
$BiOBr_xI_{1-x}$ ($0 \le x \le 1$)@PAN; $BiOBr_{0.5}I_{0.5}$@PAN	Electrospinning $Bi(NO_3)_3{\cdot}5H_2O$, Polyvinylpyrrolidone	10 mg L^{-1} MO, 0.4 g L^{-1}	Visible light	94.4% in 180 ~2.5 and 3.2 times higher than BiOBr@PAN and BiOI@PAN, respectively. $^{\cdot}O_2^-$	158
$BiOBr_xI_{1-x}$; $BiOBr_{0.3}I_{0.7}$	Ultrasonication $Bi(NO_3)_3{\cdot}5H_2O$, water	10 mg L^{-1} MO, 0.67 g L^{-1}	Visible light	92% in 40 min. Higher than pure BiOCl, BiOBr. $^{\cdot}O_2^-$ & h^+	159
$BiOCl_xI_{1-x}$ (x = 0.75)	Precipitation $Bi(NO_3)_3{\cdot}5H_2O$, nitric acid, polyvinylpyrrolidone, citric acid	20 mg L^{-1} RhB, 1 g L^{-1}	Visible light	99.2% in 80 min	160
$BiOCl_xBr_{1-x}$; BiOClBr	Precipitation $Bi(NO_3)_3{\cdot}5H_2O$, nitric acid, water	10^{-5} RhB, 0.5 g L^{-1}	Visible light	99% in 30 min ~2.0 & 6.9 times higher than BiOBr & BiOI, respectively. 3.5, 14.9	161
$BiOCl_{0.808}Br_{0.192}$/alumina	Hydrolysis & precipitation Aluminium tri-*sec*-butoxide, water $Bi(NO_3)_3{\cdot}5H_2O$, acetic acid	5 mg L^{-1} RhB	Visible light	>99.3% in 60 min $^{\cdot}O_2^-$ & $^{\cdot}OH$	162
$BiOCl_xBr_{1-x}$; $BiOCl_{0.9}Br_{0.1}$	Solvothermal $Bi(NO_3)_3{\cdot}5H_2O$, ethylene glycol	15 mg L^{-1} RhB, 0.2 g L^{-1}	UV light	44.83% in 100 min ~51.6 & 2.6 times higher than BiOBr & BiOCl, respectively. $^{\cdot}O_2^-$, $^{\cdot}OH$ & h^+	163
$BiOBr_xI_{1-x}$; $BiOBr_{0.8}I_{0.2}$	Precipitation $Bi(NO_3)_3{\cdot}5H_2O$, ethylene glycol	20 mg L^{-1} RhB, ~0.33 g L^{-1}	Visible light	99% in 90 min 1.7 & 5.4 times higher than BiOBr & BiOI, respectively. h^+	164
$BiO(Cl_xBr_{1-x})$; $BiO(Cl_{0.5}Br_{0.5})$	Hydrothermal $Bi(NO_3)_3{\cdot}5H_2O$, water	15 mg L^{-1} RhB, 0.5 g L^{-1}	Visible light	74.2% in 60 min h^+	165
$BiOBr_xI_{1-x}$; $BiOBr_{0.75}I_{0.25}$	Solvothermal $Bi(NO_3)_3{\cdot}5H_2O$, polyvinylpyrrolidone, ethylene glycol	10 mg L^{-1} RhB, 0.4 g L^{-1}	Visible light	17.9 & 3.8 times higher than BiOBr & BiOI, respectively	166

hole pair separation and stability.[80,84] Bismuth-rich $Bi_4O_5Br_xI_{2-x}$ solid solutions synthesized *via* solvothermal methods displayed optimal performance at a Br/I ratio of 1 : 1, inhibiting the recombination of photoinduced e^-/h^+ pairs and improving the photocatalytic efficiency.[85] $Bi_{24}O_{31}Cl_xBr_{10-x}$ solid solutions demonstrate enhanced photocatalytic performance relative to individual compositions, with $Bi_{24}O_{31}Cl_5Br_5$ demonstrating the highest efficiency ascribed to its favorable band gap configuration and effective charge transfer mechanisms.[88]

Nanosheet-shaped $BiOCl_{1-x}Br_x$ solid solutions, particularly $BiOCl_{0.6}Br_{0.4}$, showed excellent performance in dye degradation under visible light due to their energy band control and efficient catalysis.[145] *In situ* growth of $BiOBr_xI_{1-x}$ solid solutions on carbon fiber cloth and their incorporation into nanofibers enhanced their photocatalytic activity and stability, demonstrating their potential for environmental applications.[154] Optimized solid solutions of $BiOM_xR_{1-x}$ exhibited notable enhancements in dye removal efficiency and stability.[160] $BiOCl_xBr_{1-x}$ sheets with a Cl : Br ratio of 1 : 1 demonstrated high dye degradation activity, ascribed to the synergistic effect of photosensitization and photocatalysis.[161] Incorporating surfactants during synthesis improves the photocatalytic activity and reusability, making them advantageous for industrial applications.[159] Visible-light-responsive $BiOBr_xI_{1-x}$ solid solutions exhibit tunable band gaps and demonstrate high photocatalytic efficiency for dye degradation.[164] $BiO(Cl_xBr_{1-x})$ solid solutions displayed efficient dye degradation under visible light, emphasizing the interplay between light absorption capacity and photooxidation reactions.[165] $BiOBr_{0.75}I_{0.25}$ showed superior performance over P25 TiO_2 in degrading organic contaminants under visible light, which was ascribed to its distinctive band structure and charge separation efficiency. These studies underscore the significance of advanced photocatalytic materials in environmental remediation, offering pathways toward cleaner ecosystems and human well-being.[166]

4.3.2. Pharmaceuticals. There are a limited number of studies on the degradation of pharmaceuticals using BiOY and $Bi_xO_yY_z$ based solid solutions photocatalysis processes. Thus, there is a pressing need for further research to develop efficient techniques for treating refractory pharmaceuticals in wastewater treatment plants. Table 2 illustrates the degradation of typical pharmaceuticals using BiOY and $Bi_xO_yY_z$-based solid solutions photocatalysts. The target pharmaceuticals studied in BiOY and $Bi_xO_yY_z$ solid-solution solutions photocatalysis include ciprofloxacin (CIP),[154,167] ibuprofen, amoxicillin (AMX), tetracycline (TC),[153,154] chlortetracycline hydrochloride (CT-HCl), acetophenone (AP), ofloxacin, tetracycline hydrochloride (TC-HCl), sulfamethazine (SMT),[168] levofloxacin (LVFX),[154,165,169] and hydroxyphenylacetic acid (*p*-HPA).[96,151] Remarkably, tetracycline has emerged as the predominant pharmaceutical target in BiOY and $Bi_xO_yY_z$ solid-solution-driven photocatalysis systems. The application of pure BiOY and $Bi_xO_yY_z$ materials in the degradation of pharmaceuticals has been hindered by their high photocorrosion and high recombination of e^-/h^+ pairs.

Several solid solutions, including $BiOCl_{0.75}I_{0.25}$ and $BiOBr_{0.95}$-$I_{0.05}$, exhibit high degradation efficiencies for various pollutants, including *p*-HPA, AMX, and TC.[96,151,153] *In situ* growth of $BiOBr_x$-I_{1-x} solid solutions on carbon fiber cloth resulted in tunable bandgaps and enhanced photocatalytic activity. Notably, CFC/$BiOBr_{0.8}I_{0.2}$ showed exceptional efficiency in degrading antibiotics under visible light.[154] Additionally, (Cl : Br = 1 : 3)–U solid solution demonstrated outstanding CIP removal efficiency, attributed to its unique morphology and effective electron–hole pair separation.[167] F-doped $BiOCl_{0.4}Br_{0.3}I_{0.3}$ displayed remarkable

Table 2 Summary of the reported literature on the photocatalytic degradation of various pharmaceuticals on BiOY and $Bi_xO_yY_z$ solid solution

Solid solution material	Synthesis method	Contaminant & dosage	Irradiation source	Photocatalytic activity & active species	Ref.
$BiOCl_xI_y$; $BiOCl_{0.75}I_{0.25}$	Precipitation $Bi(NO_3)_3{\cdot}5H_2O$, ethylene glycol, water	*p*-HPA & ACTP, 0.6 g L^{-1}, 1 g L^{-1}	Solar light	~100 & 80% in 180 min $^{\cdot}O_2^-$	96
$BiOCl_{0.75}I_{0.25}$	Precipitation $Bi(NO_3)_3{\cdot}5H_2O$, ethylene glycol, water	22.8 mg L^{-1} *p*-HPA, 0.6 g L^{-1}	Simulated solar	~100% in 120 min	151
$BiOBr_xI_{1-x}$; $BiOBr_{0.95}I_{0.05}$	Precipitation $Bi(NO_3)_3{\cdot}5H_2O$, ethylene glycol	20 mg L^{-1} TC, 0.4 g L^{-1}	Visible light	85% TC in 30 min ~3.5 & 14.9 times higher than BiOBr & BiOI, respectively. $^{\cdot}O_2^-$ & h^+	153
CFC/$BiOBr_xI_{1-x}$; CFC/$BiOBr_{0.8}I_{0.2}$	Solvothermal $Bi(NO_3)_3{\cdot}5H_2O$, DMF, ethylene glycol	10 mg L^{-1} LVFX, CIP, & TC	Visible light	Levofloxacin (94.1%), CIP (94.5%), & TC (98.9%) in 120 min e^-, $^{\cdot}O_2^-$ & h^+	154
$BiO(Cl_xBr_{1-x})$; $BiO(Cl_{0.5}Br_{0.5})$	Hydrothermal $Bi(NO_3)_3{\cdot}5H_2O$, water	15 mg L^{-1} acetophenone, 0.5 g L^{-1}	Visible light	56.05% in 240 min h^+	165
BiOX (Cl : Br = 1 : 3)–U	Sono-solvothermal $Bi(NO_3)_3{\cdot}5H_2O$, ethylene glycol	50 mg L^{-1} CIP	Simulated solar light	100% in 120 min Greater than pristine BiOBr–U (74.9%) & BiOCl–U (45.9%). $^{\cdot}OH$ & h^+	167
F-$BiOCl_{0.4}Br_{0.3}I_{0.3}$ (Bi : F = 3 : 2)	Solvothermal $Bi(NO_3)_3{\cdot}5H_2O$, NaF, ethylene glycol	10 mg L^{-1} SMT, 0.5 g L^{-1}	Visible light	99.6% in 60 min 2.6 times higher than $BiOCl_{0.4}Br_{0.3}I_{0.3}$. $^{\cdot}O_2^-$ & h^+	168
$(BiOBr)_x(Bi_7O_9I_3)_{1-x}$; $(BiOBr)_{0.75}(Bi_7O_9I_3)_{0.25}$–U	Sono-solvothermal $Bi(NO_3)_3{\cdot}5H_2O$, $Bi_7O_9I_3$, ethylene glycol	50 mg L^{-1} levofloxacin, 1 g L^{-1}	Solar light	95.4% in 120 min	169

activity in sulfamethazine degradation due to its narrow band gap and unique morphology.[168] Ultrasonically fabricated $(BiOBr)_{0.75}(Bi_7O_9I_3)_{0.25}$-U exhibited high degradation efficiency for LVFX, attributed to its optimal band gap, enhanced charge transportation, and large specific surface area.[169]

4.3.3. Phenolic compounds. Phenolic compounds are extensively utilized in industrial and everyday activities and have been identified as prevalent contaminants in water sources. Owing to their inherent stability and carcinogenic properties, these compounds pose a significant risk to human health and aquatic ecosystems, causing harm and posing threats to both.[170] Table 3 illustrates the degradation of phenolic compounds by BiOY and $Bi_xO_yY_z$-based solid solutions photocatalysts. Complete degradation of phenolic compounds such as hydroquinone, 4-chlorophenol, phenol, and resorcinol over ($Bi_4O_5Br_xI_{2-x}$; Bi_4O_5BrI,),[85] ($Bi_4O_5Br_xI_{2-x}C_y$; $Bi_{2.8}C_{1.2}O_5Br_{0.5}$-$I_{1.5}$),[171] and ($BiOBr_xI_{1-x}$; $BiOBr_{0.5}I_{0.5}$),[172] and BPA over (g-C_3N_4/$BiOCl_xI_{1-x}$)[139] and ($BiOCl_xI_{1-x}$-Ovs; $BiOCl_{0.5}I_{0.5}$-Ovs)[173] have been reported. The complete degradation was attributed to the efficient segregation of photoinduced electron–hole pairs. The

Table 3 Summary of the reported literature on the photocatalytic degradation of phenolic compounds on BiOY and $Bi_xO_yY_z$ solid solution

Solid solution material	Synthesis method	Contaminant & dosage	Irradiation source	Photocatalytic activity & active species	Ref.
$Bi_4O_5Br_xI_{2-x}$; Bi_4O_5BrI	Solvothermal $Bi(NO_3)_3{\cdot}5H_2O$, polyethylene glycol	10 mg L^{-1} phenol, 0.5 g L^{-1}	Simulated solar light	~100 in 40 min ~ 6.4 & 8.5 times higher than that of pure $Bi_4O_5Br_2$ and $Bi_4O_5I_2$ h^+, $^{\cdot}O_2^-$, & e^-	85
$Bi_{24}O_{31}Cl_xBr_{10-x}$; $Bi_{24}O_{31}Cl_5Br_5$	Solvothermal $Bi(NO_3)_3{\cdot}5H_2O$, ethylene glycol	15 mg L^{-1} phenol, 0.5 g L^{-1}	Visible light	81.0% in 120 min	88
g-C_3N_4/$BiOCl_xI_{1-x}$;	Precipitation $Bi(NO_3)_3{\cdot}5H_2O$, glycerol, PVP	10 mg L^{-1}, BPA, 0.6 g L^{-1}	Visible light	~100% in 40 min h^+ & $^{\cdot}O_2^-$	139
$BiO(OH)_xI_{1-x}$; $BiO(OH)_{0.45}I_{0.55}$	Chemical precipitation $Bi(NO_3)_3{\cdot}5H_2O$, acetic acid, water	10 mg L^{-1} 2-CP, ~1.6 g L^{-1}	Visible light	88% in 40 min 10 times higher than BiOI. e^- & h^+	149
B-I_xBr_{1-x}; B–$I_{0.3}Br_{0.7}$	Microwave heating $Bi(NO_3)_3{\cdot}5H_2O$, ethylene glycol	10 mg L^{-1} 4NP, 3NP & BPA, 1 g L^{-1}	Visible light	97.5%, 72.8, & 27.5 for BPA, 4NP, & 3NP, respectively in 180 min h^+, $^{\cdot}O_2^-$, & $^{\cdot}OH$	150
$BiOBr_xI_{1-x}$; $BiOBr_{0.5}I_{0.5}$	Precipitation $Bi(NO_3)_3{\cdot}5H_2O$, ethylene glycol	10 mg BPA, 0.4 g L^{-1}	Visible light	—	153
$BiOBr_xI_{1-x}$ ($0 \le x \le 1$)@PAN; $BiOBr_{0.5}I_{0.5}$@PAN	Electrospinning $Bi(NO_3)_3{\cdot}5H_2O$, Polyvinylpyrrolidone	10 mg L^{-1} BPA, 0.4 g L^{-1}	Visible light	94.4% in 180 ~1.9 times higher than BiOI@PAN. $^{\cdot}O_2^-$ and h^+	157
$BiOBr_xI_{1-x}$; $BiOBr_{0.75}I_{0.25}$	Solvothermal $Bi(NO_3)_3{\cdot}5H_2O$, polyvinylpyrrolidone, ethylene glycol	10 mg L^{-1} BPA, 0.4 g L^{-1}	Visible light	17.3 & 2.3 times higher than BiOBr & BiOI, respectively	166
$Bi_4O_5Br_xI_{2-x}C_y$; $Bi_{2.8}C_{1.2}O_5Br_{0.5}I_{1.5}$	Solvothermal $Bi(NO_3)_3{\cdot}5H_2O$, ethylene glycol	10 mg L^{-1} phenol, 1 g L^{-1}	Visible light	100% in 60 min h^+ & $^{\cdot}O_2^-$	171
$BiOBr_xI_{1-x}$; $BiOBr_{0.5}I_{0.5}$	Solvothermal $Bi(NO_3)_3{\cdot}5H_2O$, ethylene glycol	20 mg L^{-1} phenol, 2 g L^{-1}	Visible light	100% in 80 min $^{\cdot}O_2^-$	172
$BiOCl_xI_{1-x}$-OVs; $BiOCl_{0.5}I_{0.5}$-OVs	Solvothermal $Bi(NO_3)_3{\cdot}5H_2O$, ethylene glycol, polyvinylpyrrolidone	5 mg L^{-1} BPA, 0.5 g L^{-1}	Visible light	~100% in 45 min 22.4, 3.1 and 4.5 times higher than BiOCl, BiOCl-OVs and $BiOCl_{0.5}I_{0.5}$, respectively. h^+ & $^{\cdot}O_2^-$	173
Ag–$AgCl_{0.5}Br_{0.5}$/ $BiOCl_{0.5}Br_{0.5}$	Solvothermal $Bi(NO_3)_3{\cdot}5H_2O$, $AgNO_3$, ethylene glycol	10 mg L^{-1} BPA, 0.5 g L^{-1}	Visible light	84.52% in 300 min $^{\cdot}O_2^-$, & h^+	174
Ag–AgI/AgCl/ $Bi_3O_4Cl_{0.5}Br_{0.5}$	Photo-reduction $Bi(NO_3)_3{\cdot}5H_2O$, $AgNO_3$, Bi_2O_3, absolute ethanol	10 mg L^{-1} phenol, 0.5 g L^{-1}	Visible light	57.7% in 300 min 4 & 1.5 times higher than $Bi_3O_4Cl_{0.5}Br_{0.5}$ & Ag–AgI/AgCl, respectively	175
$BiOCl_{1-x}Br_x$; $BiOCl_{0.3}Br_{0.7}$	Solvothermal $Bi(NO_3)_3{\cdot}5H_2O$, 2-methoxyethanol	10 mg L^{-1} PNP & TBBPA, 1 g L^{-1}	Visible light	98 & in 60 min & 97% in 30 min. h^+ & $^{\cdot}O_2^-$	176
$BiOBr_nI_{1-n}$; $BiOBr_{0.75}I_{0.25}$	Solvothermal $Bi(NO_3)_3{\cdot}5H_2O$, dimethylformamide, ethylene glycol	20 mg L^{-1} *p*-cresol, 1 g L^{-1}	Visible light	>99% in 90 min 31 & 1.7 times higher than pure BiOBr & BiOI, respectively. $^{\cdot}OH$, h^+, & $^{\cdot}O_2^-$	177

synergistic interaction between the solid solution and OV and a strong internal electric field facilitated this phenomenon. The unique architectural features, combining a 2D structure and dominant {0 0 1} crystal facets, also contributed to this process.

Several other studies have explored the synthesis and performance of bismuth-based solid-solution photocatalysts for phenol degradation. Liu *et al.*[88] reported enhanced phenol degradation using Bi-based solid solutions, outperforming pure $Bi_{24}O_{31}Cl_{10}$ and $Bi_{24}O_{31}Br_{10}$ owing to the improved band structures. Ji *et al.*[149] showed ten times higher degradation of 2-chlorophenol compared to BiOI, which was attributed to efficient interfacial reactions and electron migration in $BiO(OH)_x$-I_{1-x} solid solutions. Chachvalvutikul *et al.*[150] demonstrated superior activity in phenolic compound degradation using Bi_7O_9-I_3–$Bi_4O_5Br_2$ solid-solution photocatalysts with B-$I_{0.3}Br_{0.7}$, showing enhanced degradation rates and improved charge carrier separation. Liu *et al.*[158] found that $BiOBr_xI_{1-x}$@PAN nanofibers exhibited 1.9 times higher degradation of BPA than BiOI@PAN, with $BiOBr_{0.75}I_{0.25}$ (ref. 166) showing significant improvement over pure BiOBr and BiOI. Additionally, Ag–$AgCl_{0.5}Br_{0.5}$/$BiOCl_{0.5}$-$Br_{0.5}$ (ref. 174) and a polycomplex of Ag–AgI/AgCl/$Bi_3O_4Cl_{0.5}Br_{0.5}$ (ref. 175) demonstrated remarkable photocatalytic activities, attributed to synergistic effects that facilitate charge separation. Hierarchical microspheres of $BiOCl_{1-x}Br_x$ and $BiOBr_nI_{1-n}$ exhibit adjustable band gaps and high degradation efficiencies for alkyl phenols and EDCs, with $BiOBr_{0.75}I_{0.25}$ showing superior performance and sustained activity over multiple cycles.[176,177]

4.3.4. Metal ions. The global issue of heavy metal water contamination significantly threatens human health and the natural environment. Despite its known carcinogenic and mutagenic properties, hexavalent chromium (Cr(VI)) remains a key ingredient in various industrial processes, such as electroplating, leather tanning, and the production of anti-corrosion steel. Cr(III) ions are considered safe with relatively low toxicity compared to other chromium ions. Therefore, photocatalytic conversion of Cr(IV) to Cr(III) is imperative. Table 4 lists the preparation methods, contaminant dosage, percentage removal of metal ions, and reactive species involved in the reported solid solutions.

Bai *et al.*[148] highlighted the enhanced photocatalytic reduction of Cr(VI) by $BiOBr_{0.75}I_{0.25}$, attributed to band structure modification through iodine substitution for bromine, inducing defect states that facilitate electron transfer and reduce recombination.[166] Hussain *et al.*[178] demonstrated the superior photocatalytic activity of $BiOCl_{0.8}$-$Br_{0.2}$ compared to that of pure BiOCl or BiOBr, owing to its larger surface area, microporous volume, and morphology, which provide additional active sites for Cr(VI) adsorption and charge carrier transport. Wang *et al.*[179] introduced halogen vacancies into $BiOCl_{1-x}I_x$ solid solutions, resulting in broadened band structures and the creation of active sites that significantly improved the reduction of Cr(VI) ions, supported by the extended optical absorption range and effective charge carrier separation within the solid solution.

4.3.5. Air purification. Revolutionizing air purification through cutting-edge photocatalytic processes can enhance environmental sustainability and health. The breakdown of gaseous pollutants through photocatalysis primarily involves three pivotal stages: (i) separation and migration of charges, (ii) generation of reactive oxygen species (h+, $^{\bullet}OH$, and/or $^{\bullet}O_2^-$), and (iii) catalytic reduction reactions.[180] BiOY and $Bi_xO_yY_z$ solid solution photocatalysts have recently garnered significant attention in the photoreduction of NO_x, CO_2, and other gases. Table 5 lists the preparation methods, contaminant dosage, percentage removal, and reactive species involved in the reported solid solutions.

Bai *et al.*[148] emphasized the influence of conduction band position on the photocatalytic activity of bismuth-rich $Bi_4O_5Br_xI_{2-x}$ solid solutions in achieving enhanced CO_2 conversion rates. Dong *et al.*[181] demonstrated efficient removal of NO gas using BiOI/BiOCl solid solutions, with $BiOI_{0.25}Cl_{0.75}$ exhibiting superior performance owing to its 3D flower-like morphology and high surface area. Wu *et al.*[182] recorded significant oxidation of NO gas by a $BiOCl_{0.5}Br_{0.5}$ solid solution, which was attributed to its

Table 4 Summary of the reported literature on the photocatalytic reduction of various metal ions on BiOY and $Bi_xO_yY_z$ solid solution

Solid solution material	Synthesis method	Contaminant & dosage	Irradiation source	Photocatalytic activity & active species	Ref.
$BiOCl_xI_{1-x}$; $BiOCl_{0.7}I_{0.3}$ $BiOBr_xI_{1-x}$; $BiOBr_{0.7}I_{0.3}$ $BiOCl_xBr_{1-x}$; $BiOCl_{0.3}Br_{0.7}$	Solvothermal $Bi(NO_3)_3{\cdot}5H_2O$, ethylene glycol	10 mg L^{-1} Cr(VI), 1 g L^{-1}	Visible light	~100% in less than 30m min ~100% in less than 30m min 97.7% in 60 min	147
$Bi_4O_5Br_xI_{2-x}$; Bi_4O_5BrI	Hydrolytic $Bi(NO_3)_3{\cdot}5H_2O$, glycerol	60 mg L^{-1} Cr(VI), 0.4 g L^{-1}	Visible light	88% in 60 min higher than $Bi_4O_5Br_2$ (47%) & $Bi_4O_5I_2$ (53%)	148
$BiOBr_xI_{1-x}$; $BiOBr_{0.75}I_{0.25}$	Solvothermal $Bi(NO_3)_3{\cdot}5H_2O$, polyvinylpyrrolidone, ethylene glycol	10 mg L^{-1} Cr^{6+}, 0.4 g L^{-1}	Visible light	12.2 & 5.1 times higher than BiOBr & BiOI, respectively	166
$BiOCl_xBr_{1-x}$; $BiOCl_{0.8}Br_{0.2}$	Precipitation $Bi(NO_3)_3{\cdot}5H_2O$, ethylene glycol, water	8 mg L^{-1} Cr(VI), 0.5 g L^{-1}	Visible light	$BiOCl_{0.8}Br_{0.2}$ showed higher photocatalytic activity than pure BiOCl or BiOBr	178
$BiOCl_{1-n}I_n$; $BiOCl_{0.6}I_{0.4}$	Solvothermal $Bi(NO_3)_3{\cdot}5H_2O$, glycerol, water	35 mg L^{-1}, Cr(VI)	UV-vis	87.7 in 35 min	179

Table 5 Summary of the reported literature on the photocatalytic degradation of various gaseous compounds on BiOY and $Bi_xO_yY_z$ solid solution

Solid solution material	Synthesis method	Contaminant & dosage	Irradiation source	Photocatalytic activity & active species	Ref.
$Bi_4O_5Br_xI_{2-x}$; Bi_4O_5BrI	Hydrolytic $Bi(NO_3)_3{\cdot}5H_2O$, glycerol	CO_2	Visible light	0.372% in 240 min 3.65 & 2.72 time higher than $Bi_4O_5Br_2$ (0.102%) and $Bi_4O_5I_2$ (0.137%), respectively	148
$BiOI_{0.25}Cl_{0.75}$	Template free $Bi(NO_3)_3{\cdot}5H_2O$, water	450 ppb NO	Simulated solar light	54.6% in 30 min 21 & 4 times higher than BiOCl & BiOI, respectively	181
$BiOCl_xBr_{1-x}$; $BiOCl_{0.5}Br_{0.5}$	Template free $Bi(NO_3)_3{\cdot}5H_2O$, water	100 ppm NO	Visible light	57.3% in 40 min 3 & 19 times higher than BiOBr & BiOCl, respectively. $^{\cdot}OH$ & $^{\cdot}O_2^-$	182
$Bi_3O_4Cl_xBr_{1-x}$; $Bi_3O_4Cl_{0.5}Br_{0.5}$	Solid state reaction $Bi(NO_3)_3{\cdot}5H_2O$, Bi_2O_3, ethylene glycol	600 ppb NO	Simulated visible light	60% in 10 min. Greater than Bi_3O_4Cl (25%) and Bi_3O_4Br (35%). h^+	183
$(BiO)_2(CO_3)_x(I_2)_{1-x}$; $(BiO)_2(CO_3)_{0.75}(I_2)_{0.25}$	Precipitation $Bi(NO_3)_3{\cdot}5H_2O$, $(BiO)_2CO_3$, nitric acid	600 ppb NO	Visible light	50.8% in 30 min. 50 & 8 times higher than pure $(BiO)_2CO_3$ & BiOI, respectively	184
$BiOBr_xCl_{1-x}$; $BiOBr_{0.6}Cl_{0.4}$	Precipitation $Bi(NO_3)_3{\cdot}5H_2O$, nitric acid	CO_2 reduction to CO and O_2	Simulated solar light	7.5 and 10.2 times higher than pure BiOCl & BiOBr, respectively	185

hierarchical nanostructures and modified band structures. Similarly, Bai *et al.*[183] reported enhanced NO degradation by a $Bi_3O_4Cl_{0.5}Br_{0.5}$ solid solution owing to efficient charge separation. Ou *et al.*[184] highlighted the remarkable NO degradation efficiency of a $(BiO)_2(CO_3)_{0.75}(I_2)_{0.25}$ solid solution, attributed to its tailored band structure and hierarchical morphology. Gao *et al.*[185] synthesized Persian buttercup-like $BiOBr_{0.6}Cl_{0.4}$, which exhibited notable CO_2 photoreduction rates and outstanding stability over multiple cycles.

4.3.6. Other pollutants. Contemporary environmental pollution from pollutants including formaldehyde, sodium pentachlorophenate, bacteria, acrylamide, naphthalene, and trace organic pollutants (TrOPs) presents significant challenges to both the environment and human health. Understanding their degradation mechanisms and assessing the efficacy of photocatalytic treatment is crucial for devising effective remediation strategies. Numerous studies have reported the degradation of these pollutants using photocatalysts based on BiOY and $Bi_xO_yY_z$ solid solutions.[186] Despite employing different methodologies and materials, these studies aim to enhance the photocatalytic activity for environmental remediation. The removal of these other pollutants is summarized in Table 6.

Highly stable composite films ($BiOCl_{0.808}Br_{0.192}$/alumina) achieved complete naphthalene degradation within 60 min.[159] The development of BiOY nanostructures (Ag–$AgCl_{0.5}Br_{0.5}$/$BiOCl_{0.5}Br_{0.5}$ and Ag–AgI/AgCl/$Bi_3O_4Cl_{0.5}Br_{0.5}$) has expanded applications to acrylamide and bisphenol A degradation, with elemental bismuth doping enhancing organic contaminant mineralization.[174,175] Dandapat *et al.*[187] engineered Bi(0)-doped BiOY solid solution films, notably 3% Bi(0)-doped $BiOCl_{0.875}Br_{0.125}$, exhibiting enhanced TrOPs degradation due to ion-exchange adsorption mechanisms. Similarly, UV light-induced OVs on $BiOCl_{0.95}Br_{0.05}$-010-OVs enhanced PCPNa degradation and remained stable over time for long-term applications.[188] Controlled doping of $BiOCl_xBr_{1-x}$ solid solution with elemental bismuth particles enhances the mineralization of various pollutants, fully decomposing toluene, chlorobenzene, xylene, and benzene into CO_2 and water.[189] The $BiOBr_{0.75}I_{0.25}$ nanostructures displayed high bactericidal activity, suggesting potential beyond photocatalysis for environmental challenges.[186]

5. Challenges and recommendations

Although BiOY and $Bi_xO_yY_z$ photocatalysts have been extensively studied, there remain some inherent challenges that should be addressed for the full exploitation of these materials in various fields.

1. Optimizing the synthesis methods for practical scalability is crucial. The current laboratory-scale synthesis methods for BiOY and $Bi_xO_yY_z$ photocatalysts involve multistep reactions with low yields and long reaction times. It is essential to develop simpler, more efficient, and scalable methods suitable for commercial applications.

2. Expanding the applications for energy conversion is a priority. BiOY and $Bi_xO_yY_z$ photocatalysts are primarily used for organic contaminant degradation and heavy metal removal, with limited research on energy conversion processes, such as CO_2 reduction and water splitting. Enhancing the photocatalytic efficiency, stability, and bandgap adjustment can broaden their applicability in energy-related fields.

3. Enhancing recyclability and understanding environmental impacts are key considerations. Recyclability is essential for the practical application of BiOY and $Bi_xO_yY_z$, ensuring greenness, safety, and economic feasibility. Assessing the environmental impact of the synthesis and modification processes is necessary, including the evaluation of potential ecological risks and ecotoxicological effects.

4. Clarifying the reaction mechanisms and exploring theoretical simulations are critical. The exact reaction mechanisms of BiOY and $Bi_xO_yY_z$ and their nanocomposites remain unclear, particularly in multi-step reactions and electron transfer processes. Utilizing *in situ* spectroscopy and theoretical

Table 6 Summary of the reported literature on the photocatalytic degradation of various other pollutants on BiOY and $Bi_xO_yY_z$ solid solution

Solid solution material	Synthesis method	Contaminant & dosage	Irradiation source	Photocatalytic activity & active species	Ref.
$BiOCl_{0.808}Br_{0.192}$/alumina	Hydrolysis & precipitation. Aluminium tri-*sec*-butoxide, water $Bi(NO_3)_3{\cdot}5H_2O$, acetic acid	25 mg L^{-1} naphthalene	Visible light	~100% in 60 min	159
Ag–AgI/AgCl/ $Bi_3O_4Cl_{0.5}Br_{0.5}$	Photo-reduction $Bi(NO_3)_3{\cdot}5H_2O$, $AgNO_3$, Bi_2O_3, absolute ethanol	10 mg L^{-1} acrylamide, 0.5 g L^{-1}	UV light	41.0% in 300 min 3.1 & 1.6 times higher than $Bi_3O_4Cl_{0.5}Br_{0.5}$ & Ag–AgI/AgCl, respectively	175
Ag–$AgCl_{0.5}Br_{0.5}$/ $BiOCl_{0.5}Br_{0.5}$	Solvothermal $Bi(NO_3)_3{\cdot}5H_2O$, $AgNO_3$, ethylene glycol	10 mg L^{-1} acrylimide, 0.5 g L^{-1}	Visible light	75.63% in 300 min $^{\bullet}O_2^-$, & h^+	174
$BiOBr_xI_{1-x}$; $BiOBr_{0.75}I_{0.25}$	Precipitation $Bi(NO_3)_3{\cdot}5H_2O$, acetic acid	10^9 CFU mL^{-1} *Escherichia coli*, 15 mg L^{-1} 10^6 CFU mL^{-1} *Bacillus subtilis*, 10 mg L^{-1}	Visible light	~100% in 10 min ~100% in 120 min	186
3% Bi(0)-doped $BiOCl_{0.875}Br_{0.125}$	Precipitation $Bi(NO_3)_3{\cdot}5H_2O$, acetic acid, water, CTAB	100 μg L^{-1} TrOPs (CBZ, VLX, & BZF)	Solar simulator	Degradation followed the order BZF > VLX > CBZ	187
$BiOCl_{0.95}Br_{0.05}$	Hydrothermal $Bi(NO_3)_3{\cdot}5H_2O$, water	15 mg L^{-1} PCPNa, 1 g L^{-1}	UV light		188
$BiOCl_xBr_{1-x}$; 3% Bi-doped $BiOCl_{0.875}Br_{0.125}$	Precipitation $Bi(NO_3)_3{\cdot}5H_2O$, acetic acid, sodium borohydride	Chlorobenzene, benzene, toluene, xylene, 0.75 g L^{-1}	Visible light	Fully decomposed to CO_2 & H_2O	189

simulations, such as DFT can deepen our understanding of structure–activity relationships and reaction pathways.

5. A notable challenge identified in the reviewed studies is the need for reported degradation products. Despite the extensive research on environmental pollutants, many studies need to provide comprehensive information regarding the degradation by-products, hindering a thorough understanding of the pollutant's fate and potential environmental impact.

6. Conclusions and perspectives

The distinctive layered structure and adjustable electronic properties of BiOX and $Bi_xO_yY_z$ make them promising candidates for environmental remediation. Pure BiOX and $Bi_xO_yY_z$ face inherent limitations, such as inadequate light absorption, insufficient surface-active sites, and an inclination for fast recombination of e^-/h^+ pairs. Many optimized structural strategies have emerged to mitigate these environmental challenges, ushering in a new realm of possibilities for enhancing photocatalytic performance. The improvement of photocatalytic efficiency in pure BiOY and $Bi_xO_yY_z$ is primarily achieved through solid solution formation, which involves adjusting the energy band structure and influencing carrier dynamics. The photocatalytic efficacy of BiOY and $Bi_xO_yY_z$ solid solutions depends on their specific compositions. Fine-tuning of the energy band structure was accomplished by modifying the halogen composition. With an increase in the proportion of halogens possessing more significant atomic numbers, the VB position progressively increases, constricting the bandgap width of the catalyst and substantially augmenting light absorption. This results in a more substantial generation of photogenerated carriers. Conversely, the elevated VB position diminishes the redox capability of the charge carriers.

Moreover, solid solution-based materials derived from BiOY and $Bi_xO_yY_z$ have found applications in the removal of dyes, phenolic compounds, metal ions, pharmaceuticals, and air (NO_2 and CO_2) reduction, showing commendable photocatalytic efficacy and operational stability. Enhanced characterization methodologies hold the promise of offering novel insights into structural evolution and gaining a comprehensive understanding of photocatalytic processes. Currently, characterization techniques predominantly rely on *ex situ* methods.

BiOY and $Bi_xO_yY_z$ stand out as exceptional layered materials characterized by outstanding photochemical attributes with immense promise for significant advancements in diverse environmental applications. However, evaluating BiOY and $Bi_xO_yY_z$-based photodegradation processes predominantly focuses on aqueous solutions, leaving a notable absence of studies concerning gaseous pollutants, particularly volatile organic compounds. Further, there is a pressing need to develop robust methodologies for monitoring the toxicity of photocatalytic end products during the treatment of complex organic contaminants to mitigate the risk of secondary pollution. Lastly, this review has shed light on improving the intrinsic properties of BiOY and $Bi_xO_yY_z$-based solid solutions. Such insights are expected to propel and diversify the applications of bismuth-based photocatalysts.

Data availability

This review paper synthesizes data from previously published studies. No new data were generated or analyzed in this study. All data supporting the findings of this review are available from the corresponding publications cited in the reference section. The datasets analyzed during the review

are publicly accessible and can be found in the respective repositories as mentioned in the original studies.

Author contributions

Robert O. Gembo: conceptualization, methodology, data collection, data analysis, data curation, writing – original draft; Rudzani Ratshiedana: writing – review and editing; Alex T. Kuvarega: writing – review and editing; Lawrence M. Madikizela: supervision, writing – review and editing; I. Kamika: supervision, writing – review and editing; Cecil K. King'ondu: writing – review and editing; and Titus A. M. Msagati: conceptualization, resources, funding, supervision, writing – review and editing.

Conflicts of interest

The authors declare that they have no known competing financial interests or personal relationships that could have influenced the work reported in this study.

Acknowledgements

The authors would like to express their sincere gratitude to Dr Orlette Mkhari for his invaluable contributions to the manuscript. Additionally, they acknowledge the Institute for Nanotechnology and Water Sustainability and University of South Africa (UNISA) for administrative support.

References

1 K. A. Adegoke, O. R. Adegoke, R. A. Adigun, N. W. Maxakato and O. S. Bello, Two-dimensional metal-organic frameworks: From synthesis to biomedical, environmental, and energy conversion applications, *Coord. Chem. Rev.*, 2022, **473**, 214817.

2 J. Z. Hassan, A. Raza, U. Qumar and G. Li, Recent advances in engineering strategies of Bi-based photocatalysts for environmental remediation, *Sustainable Mater. Technol.*, 2022, **33**, e00478.

3 A. Kumar, G. Sharma, Mu. Naushadd, A. H. Al-Muhtaseb, A. García-Peñas, G. T. Molaf, C. Si and F. J. Stadler, Bio-inspired and biomaterials-based hybrid photocatalysts for environmental detoxification: A review, *Chem. Eng. J.*, 2020, **382**, 122937.

4 R. O. Gembo, O. Aoyi, S. Majoni, A. Etale, S. Odisitse and C. K. King'ondu, Synthesis of bismuth oxyhalide ($BiOBr_zI_{(1-z)}$) solid solutions for photodegradation of methylene blue dye, *AAS Open Res.*, 2022, **4**, 43.

5 J. Sharma, P. Dhiman, R. A. Alshgari, Z. A. ALOthman, A. Kumar, G. Sharma and G. Rana, Advances in photocatalytic environmental and clean energy applications of bismuth-rich oxy halides-based heterojunctions: a review, *Mater. Today Sustain.*, 2023, **21**, 100327.

6 N. Tian, C. Hu, J. Wang, Y. Zhang, T. Ma and H. Huang, Layered bismuth-based photocatalysts, *Coord. Chem. Rev.*, 2022, **463**, 214515.

7 A. Fujishima and K. Honda, Electrochemical Photolysis of Water at a Semiconductor Electrode, *Nature*, 1972, **238**(5358), 37–38.

8 R. Asahi, T. Morikawa, H. Irie and T. Ohwaki, Nitrogen-doped titanium dioxide as visible-light-sensitive photocatalyst: Designs, developments, and prospects, *Chem. Rev.*, 2014, **114**(19), 9824–9852.

9 A. Kudo and Y. Miseki, Heterogeneous photocatalyst materials for water splitting, *Chem. Soc. Rev.*, 2009, **38**(1), 253–278.

10 P. Zhang, J. Zhang and J. Gong, Tantalum-based semiconductors for solar water splitting, *Chem. Soc. Rev.*, 2014, **43**(13), 4395–4422.

11 G. Liu, P. Niu and H. M. Cheng, Visible-light-active elemental photocatalysts, *ChemPhysChem*, 2013, **14**(5), 885–892.

12 N. Zhang, R. Ciriminna, M. Pagliaro and Y. J. Xu, Nanochemistry-derived Bi_2WO_6 nanostructures: Towards production of sustainable chemicals and fuels induced by visible light, *Chem. Soc. Rev.*, 2014, **43**(15), 5276–5287.

13 L. Zhang and Y. Zhu, A review of controllable synthesis and enhancement of performances of bismuth tungstate visible-light-driven photocatalysts, *Catal. Sci. Technol.*, 2012, **2**(4), 694–706.

14 J. Yang, Z. Huang, J. Li, Y. Yao, Y. Meng, B. Xie, Z. Ni and S. Xia, Photocatalytic reduction of nitrogen to ammonia by bismuth oxyhalides containing oxygen vacancies, *Colloids Surf., A*, 2023, **662**(11), 130995.

15 Y. Sun, Y. Ahmadi, K. H. Kim and J. Lee, The use of bismuth-based photocatalysts for the production of ammonia through photocatalytic nitrogen fixation, *Renewable Sustainable Energy Rev.*, 2022, **170**(6), 112967.

16 M. Arumugam, T. S. Natarajan, T. Saelee, S. Praserthdam, M. Ashokkumar and P. Praserthdam, Recent developments on bismuth oxyhalides (BiOX; X = Cl, Br, I) based ternary nanocomposite photocatalysts for environmental applications, *Chemosphere*, 2021, **282**(6), 131054.

17 Z. Mengting, T. A. Kurniawan, L. Duan, Y. Song, S. W. Hermanowicz and M. H. D. Othman, Advances in BiOX-based ternary photocatalysts for water technology and energy storage applications: Research trends, challenges, solutions, and ways forward, *Rev. Environ. Sci. Biotechnol.*, 2022, **21**, 331–370.

18 S. Liu, J. Sun, G. Ren and X. Meng, Vacancy-engineered bismuth-based semiconductor with enhanced photocatalytic activity: A review, *Mater. Sci. Semicond. Process.*, 2022, **137**, 106230.

19 Z. Wang, M. Chen, D. Huang, G. Zeng, P. Xu, C. Zhou, H. Lai, M. Wang and W. W. Cheng, Multiply structural optimized strategies for bismuth oxyhalide photocatalysis and their environmental application, *Chem. Eng. J.*, 2019, **374**(6), 1025–1045.

20 I. Ahmad, S. Shukrullah, M. Yasin Naz, S. Ullah and A. M. Ali, Designing and modification of bismuth oxyhalides BiOX (X = Cl, Br and I) photocatalysts for improved photocatalytic performance, *J. Ind. Eng. Chem.*, 2022, **105**(9), 1–33.

21 J. Xiong, P. Song, J. Di and H. Li, Bismuth-rich bismuth oxyhalides: A new opportunity to trigger high-efficiency photocatalysis, *J. Mater. Chem. A*, 2020, **8**(41), 21434–21454.
22 L. Wang, L. Wang, Y. Du, X. Xu and S. X. Dou, Progress and perspectives of bismuth oxyhalides in catalytic applications, *Mater. Today Phys.*, 2021, **16**, 100294.
23 A. Malathi, J. Madhavan, M. Ashokkumar and P. Arunachalam, A review on $BiVO_4$ photocatalyst: Activity enhancement methods for solar photocatalytic applications, *Appl. Catal., A*, 2018, **555**, 47–74.
24 G. A. Kallawar, D. P. Barai and B. A. Bhanvase, Bismuth titanate based photocatalysts for degradation of persistent organic compounds in wastewater: A comprehensive review on synthesis methods, performance as photocatalyst and challenges, *J. Cleaner Prod.*, 2021, **318**, 128563.
25 A. Elaouni, M. El Ouardi, A. BaQais, M. Arab, M. Saadi and H. Ait Ahsaine, Bismuth tungstate Bi_2WO_6: a review on structural, photophysical and photocatalytic properties, *RSC Adv.*, 2023, **13**(26), 17476–17494.
26 M. Shetty, K. Manickavasakam, N. Kulal, P. D. Shivaramu, M. N. Rani, M. Shastri, M. Murthy, S. J. Babu, G. V. Shanbhag, M. Sathish and D. Rangapp, Bismuth oxycarbonate Nanoplates@α-$Ni(OH)_2$ nanosheets 2D plate-on-sheet heterostructure as electrode for high-performance supercapacitor, *J. Alloys Compd.*, 2021, **860**, 158495.
27 H. R. Mahmoud, Bismuth silicate ($Bi_4Si_3O_{12}$ and Bi_2SiO_5) prepared by ultrasonic-assisted hydrothermal method as novel catalysts for biodiesel production via oleic acid esterification with methanol, *Fuel*, 2019, **256**, 115979.
28 N. Wang, X. Luo, L. Han, Z. Zhang, R. Zhang, H. Olin and Y. Yang, Structure, Performance, and Application of $BiFeO_3$ Nanomaterials, *Nano-Micro Lett.*, 2020, **12**(1), 81.
29 G. Yang, Y. Liang, K. Li, J. Yang, K. Wang, R. Xu and X. Xie, Engineering the dimension and crystal structure of bismuth molybdate photocatalysts via a molten salt-assisted assembly approach, *J. Alloys Compd.*, 2020, **844**, 156231.
30 Y. Liu, Z. Zhu, Y. Liu, J. Wu, Y. Ling, Z. Xiang, S. Qin, Y. Ye and M. Bai, First principles insight on enhanced photocatalytic performance of sulfur-doped bismuth oxide iodate, *Mater. Sci. Semicond. Process.*, 2023, **165**, 107672.
31 M. Kuznetsova, S. A. A. Oliveira, B. S. Rodrigues and J. S. Souza, Microwave-Assisted Synthesis of Bismuth Niobate/Tungsten Oxide Photoanodes for Water Splitting, *Top. Catal.*, 2021, **64**(13–16), 748–757.
32 R. Kumar, P. Raizada, A. A. P. Khan, V. H. Nguyen, Q. Van Le, S. Ghotekar, R. Selvasembian, V. Gandhi, A. Singh and P. Singh, Recent progress in emerging $BiPO_4$-based photocatalysts: Synthesis, properties, modification strategies, and photocatalytic applications, *J. Mater. Sci. Technol.*, 2022, **108**, 208–225.
33 R. He, D. Xu, B. Cheng, J. Yu and W. Ho, Review on nanoscale Bi-based photocatalysts, *Nanoscale Horiz.*, 2018, **3**(5), 464–504.
34 J. Di, C. Zhu, M. Ji, M. Duan, R. Long, C. Yan, K. Gu, J. Xiong, Y. She, J. Xia, H. Li and Z. Liu, Defect-Rich $Bi_{12}O_{17}Cl_2$ Nanotubes Self-Accelerating Charge Separation for Boosting Photocatalytic CO_2 Reduction, *Angew. Chem., Int. Ed.*, 2018, **57**(45), 14847–14851.
35 P. Gao, Y. Yang, Z. Yin, F. Kang, W. Fan, J. Sheng, L. Feng, Y. Liu, Z. Du and L. Zhang, A critical review on bismuth oxyhalide based photocatalysis for pharmaceutical active compounds degradation: Modifications, reactive sites, and challenges, *J. Hazard. Mater.*, 2021, **412**, 125186.
36 X. Wei, M. U. Akbar, A. Raza and G. Li, A review on bismuth oxyhalide based materials for photocatalysis, *Nanoscale Adv.*, 2021, **3**(12), 3353–3372.
37 J. Zhao, Z. Miao, Y. Zhang, G. Wen, L. Liu, X. Wang, X. Cao and B. Wang, Oxygen vacancy-rich hierarchical BiOBr hollow microspheres with dramatic CO_2 photoreduction activity, *J. Colloid Interface Sci.*, 2021, **593**, 231–243.
38 X. Ren, M. Gao, Y. Zhang, Z. Zhang, X. Cao, B. Wang and X. Wang, Photocatalytic reduction of CO_2 on BiOX: Effect of halogen element type and surface oxygen vacancy mediated mechanism, *Appl. Catal., B*, 2020, **274**, 119063.
39 J. Di, C. Chen, C. Zhu, P. Song, J. Xiong, M. Ji, J. Zhou, Q. Fu, M. Xu, W. Hao, J. Xia, S. Li, H. Li and Z. Liu, Bismuth Vacancy-Tuned Bismuth Oxybromide Ultrathin Nanosheets toward Photocatalytic CO_2 Reduction, *ACS Appl. Mater. Interfaces*, 2019, **11**(34), 30786–30792.
40 H. Yu and Q. Han, Effect of reaction mediums on photocatalytic performance of BiOX (X = Cl, Br, I), *Opt. Mater.*, 2021, **119**, 111399.
41 Y. Huang, H. Li, M. S. Balogun, W. Liu, Y. Tong, X. Lu and H. Ji, Oxygen vacancy induced bismuth oxyiodide with remarkably increased visible-light absorption and superior photocatalytic performance, *ACS Appl. Mater. Interfaces*, 2014, **6**(24), 22920–22927.
42 S. Weng, Z. Fang, Z. Wang, Z. Zheng, W. Feng and P. Liu, Construction of teethlike homojunction BiOCl (001) nanosheets by selective etching and its high photocatalytic activity, *ACS Appl. Mater. Interfaces*, 2014, **6**(21), 18423–18428.
43 H. Huang, X. Han, X. Li, S. Wang, P. K. Chu and Y. Zhang, Fabrication of multiple heterojunctions with tunable visible-light-active photocatalytic reactivity in BiOBr-BiOI full-range composites based on microstructure modulation and band structures, *ACS Appl. Mater. Interfaces*, 2015, **7**(1), 482–492.
44 Z. K. Tang, W. J. Yin, L. Zhang, B. Wen, D. Y. Zhang, L. M. Liu and W. M. Lau, Spatial separation of photo-generated electron-hole pairs in BiOBr/BiOI bilayer to facilitate water splitting, *Sci. Rep.*, 2016, **6**, 1–9.
45 C. Lai, M. Zhang, B. Li, D. Huang, G. Zeng, L. Qin, X. Liu, H. Yi, M. Cheng, L. Li, Z. Chen and L. Chen, Fabrication of CuS/$BiVO_4$ (0 4 0) binary heterojunction photocatalysts with enhanced photocatalytic activity for Ciprofloxacin degradation and mechanism insight, *Chem. Eng. J.*, 2019, **358**, 891–902.
46 R. Dong, Y. Hu, Y. Wu, W. Gao, B. Ren, Q. Wang and Y. Cai, Visible-light-driven BiOI-based janus micromotor in pure water, *J. Am. Chem. Soc.*, 2017, **139**(5), 1722–1725.

47 D. Kandi, S. Martha, A. Thirumurugan and K. M. Parida, Modification of BiOI Microplates with CdS QDs for Enhancing Stability, Optical Property, Electronic Behavior toward Rhodamine B Decolorization, and Photocatalytic Hydrogen Evolution, *J. Phys. Chem. C*, 2017, **121**(9), 4834–4849.

48 J. Hu, W. Fan, W. Ye, C. Huang and X. Qiu, Insights into the photosensitivity activity of BiOCl under visible light irradiation, *Appl. Catal., B*, 2014, **158–159**, 182–189.

49 S. O. Ganiyu, C. A. Martínez-Huitle and M. A. Rodrigo, Renewable energies driven electrochemical wastewater/soil decontamination technologies: A critical review of fundamental concepts and applications, *Appl. Catal., B*, 2020, **270**, 118857.

50 A. Sudhaik, P. Raizada, P. Shandilya, D. Y. Jeong, J. H. Lim and P. Singh, Review on fabrication of graphitic carbon nitride based efficient nanocomposites for photodegradation of aqueous phase organic pollutants, *J. Ind. Eng. Chem.*, 2018, **67**, 28–51.

51 K. L. Zhang, C. M. Liu, F. Q. Huang, C. Zheng and W. D. Wang, Study of the electronic structure and photocatalytic activity of the BiOCl photocatalyst, *Appl. Catal., B*, 2006, **68**, 125–129.

52 J. Bai, J. Sun, X. Zhu, J. Liu, H. Zhang, X. B. Yin and L. Liu, Enhancement of Solar-Driven Photocatalytic Activity of BiOI Nanosheets through Predominant Exposed High Energy Facets and Vacancy Engineering, *Small*, 2020, **16**(5), 1904783.

53 Z. Luo, X. Ye, S. Zhang, S. Xue, C. Yang, Y. Hou, W. Xing, R. Yu, J. Sun, Z. Yu and X. Wang, Unveiling the charge transfer dynamics steered by built-in electric fields in BiOBr photocatalysts, *Nat. Commun.*, 2022, **13**(1), 1–10.

54 M. Guan, C. Xiao, J. Zhang, S. Fan, R. An, Q. Cheng, J. Xie, M. Zhou, B. Ye and V. Xie, Vacancy associates promoting solar-driven photocatalytic activity of ultrathin bismuth oxychloride nanosheets, *J. Am. Chem. Soc.*, 2013, **135**(28), 10411–10417.

55 L. Sun, L. Xiang, X. Zhao, C. J. Jia, J. Yang, Z. Jin, X. Cheng and W. Fan, Enhanced visible-light photocatalytic activity of BiOI/BiOCl heterojunctions: Key role of crystal facet combination, *ACS Catal.*, 2015, **5**(6), 3540–3551.

56 X. J. Guo, M. Zhen, H. Liu and L. Liu, BiOBr-BiOI microsphere assembled with atom-thick ultrathin nanosheets and its high photocatalytic activity, *RSC Adv.*, 2015, **5**(31), 24777–24782.

57 J. Jiang, K. Zhao, X. Xiao and L. Zhang, Synthesis and facet-dependent photoreactivity of BiOCl single-crystalline nanosheets, *J. Am. Chem. Soc.*, 2012, **134**(10), 4473–4476.

58 Z. Fan, Y. Zhao, W. Zhai, L. Qiu, H. Li and M. R. Hoffmann, Facet-dependent performance of BiOBr for photocatalytic reduction of Cr(VI), *RSC Adv.*, 2016, **6**(3), 2028–2031.

59 L. Ye, X. Jin, C. Liu, C. Ding, H. Xie, K. H. Chu and P. K. Wong, Thickness-ultrathin and bismuth-rich strategies for BiOBr to enhance photoreduction of CO_2 into solar fuels, *Appl. Catal., B*, 2016, **187**, 281–290.

60 L. Wang, J. Shang, W. Hao, S. Jiang, S. Huang, T. Wang, Z. Sun, Y. Du, S. Dou, T. Xie, D. Wang and J. Wang, A dye-sensitized visible light photocatalyst-$Bi_{24}O_{31}Cl_{10}$, *Sci. Rep.*, 2014, **4**, 7384.

61 J. Li, H. Li, G. Zhan and L. Zhang, Solar water splitting and nitrogen fixation with layered bismuth oxyhalides, *Acc. Chem. Res.*, 2017, **50**(1), 112–121.

62 X. Lin, H. Tao, H. Fuqiang, W. Wendeng and S. Jianlin, Photocatalytic activity of a Bi-based oxychloride Bi_3O_4Cl, *J. Phys. Chem. B*, 2006, **110**(48), 24629–24634.

63 X. Jin, L. Ye, H. Xie and G. Chen, Bismuth-rich bismuth oxyhalides for environmental and energy photocatalysis, *Coord. Chem. Rev.*, 2017, **349**(9), 84–101.

64 A. Hussain, J. Hou, M. Tahir, S. S. Ali, Z. U. Rehman, M. Bilal, T. Zhang, Q. Dou and X. Wang, Recent advances in BiOX-based photocatalysts to enhanced efficiency for energy and environment applications, *Catal. Rev.: Sci. Eng.*, 2024, **66**(1), 119–173.

65 Y. L. Qi, G. Han and X. C. Song, Enhanced photocatalytic degradation of phenol over Ag_3PO_4-$BiOCl_{1-x}Br_x$ composites, *Mater. Res. Bull.*, 2018, **102**, 16–23.

66 J. Wang, H. Li, X. Yan, C. Qian, Y. Xing, S. Yang, Z. Kang, J. Han, W. Gu, H. Yang and F. Xiao, Synergistic enhancement of the visible-light photocatalytic activity of hierarchical 3D $BiOCl_xBr_{1-x}$/graphene oxide heterojunctions for formaldehyde degradation at room temperature, *J. Alloys Compd.*, 2019, **795**, 120–133.

67 H. Huang, C. Zeng, K. Xiao and Y. Zhang, Coupling of solid-solution and heterojunction in a 2D-1D core-shell-like $BiOCl_{0.5}I_{0.5}$/Bi_5O_7I hierarchy for promoting full-spectrum photocatalysis and molecular oxygen activation, *J. Colloid Interface Sci.*, 2017, **504**, 257–267.

68 Y. Wang, J. Meng, S. Jing, K. Wang, C. Ban, Y. Feng, Y. Duan, J. Ma, L. Gan and V. Zhou, Origin of Bismuth-Rich Strategy in Bismuth Oxyhalide Photocatalysts, *Energy Environ. Mater.*, 2023, **6**(5), 2–9.

69 C. Y. Wang, X. Zhang and H. Q. Yu, Bismuth oxyhalide photocatalysts for water purification: Progress and challenges, *Coord. Chem. Rev.*, 2023, **493**(7), 215339.

70 V. Charles, I. P. Ebuka and N. A. Gaya, Solid-Solutions as Supports and Robust Photocatalysts and Electrocatalysts: A Review, *Catal. Sustainable Energy*, 2020, **7**, 8–28.

71 R. Li and C. Li, Photocatalytic Water Splitting on Semiconductor-Based Photocatalysts, *Advances in Catalysis*, Elsevier Inc., 1st edn, 2017, vol. 60, pp. 1–57.

72 H. Shi, W. Ming and M. H. Du, Bismuth chalcohalides and oxyhalides as optoelectronic materials, *Phys. Rev. B*, 2016, **93**(10), 104108.

73 D. Gogoi, A. K. Shah, M. Qureshi, A. K. Golder and N. R. Peela, Silver grafted graphitic-carbon nitride ternary hetero-junction Ag/gC_3N_4(Urea)-gC_3N_4(Thiourea) with efficient charge transfer for enhanced visible-light photocatalytic green H_2 production, *Appl. Surf. Sci.*, 2021, **558**(2), 149900.

74 J. Di, J. Xia, H. Li, S. Guo and S. Dai, Bismuth oxyhalide layered materials for energy and environmental applications, *Nano Energy*, 2017, **41**, 172–192.

75 R. Marschall, Semiconductor composites: Strategies for enhancing charge carrier separation to improve photocatalytic activity, *Adv. Funct. Mater.*, 2014, **24**(17), 2421–2440.
76 R. Pode, Organic light emitting diode devices: An energy efficient solid state lighting for applications, *Renewable Sustainable Energy Rev.*, 2020, **133**, 110043.
77 D. Zhang, G. Li, H. Li and Y. Lu, The development of better photocatalysts through composition- and structure-engineering, *Chem. – Asian J.*, 2013, **8**, 26–40.
78 H. Y. Xu, X. Han, Q. Tan, X. L. He and S. Y. Qi, Structure-dependent photocatalytic performance of $BiOBr_xI_{1-x}$ nanoplate solid solutions, *Catalysts*, 2017, **7**(5), 153.
79 H. Zhang, L. Liu and Z. Zhou, Towards better photocatalysts: First-principles studies of the alloying effects on the photocatalytic activities of bismuth oxyhalides under visible light, *Phys. Chem. Chem. Phys.*, 2012, **14**(3), 1286–1292.
80 Y. Liu, W. J. Son, J. Lu, B. Huang, Y. Dai and M. H. Whangbo, Composition dependence of the photocatalytic activities of $BiOCl_{1-x}Br_x$ solid solutions under visible light, *Chem. – Eur. J.*, 2011, **17**(34), 9342–9349.
81 S. Ouyang and J. Ye, β-$AgAl_{1-x}Ga_xO_2$ solid-solution photocatalysts: Continuous modulation of electronic structure toward high-performance visible-light photoactivity, *J. Am. Chem. Soc.*, 2011, **133**(20), 7757–7763.
82 Q. Wang, Z. Liu, D. Liu, G. Liu, M. Yang, F. Cui and W. Wang, Ultrathin two-dimensional $BiOBr_xI_{1-x}$ solid solution with rich oxygen vacancies for enhanced visible-light-driven photoactivity in environmental remediation, *Appl. Catal., B*, 2018, **236**, 222–232.
83 H. Gnayem and Y. Sasson, Hierarchical nanostructured 3D flowerlike $BiOCl_xBr_{1-x}$ semiconductors with exceptional visible light photocatalytic activity, *ACS Catal.*, 2013, **3**(2), 186–191.
84 J. Yang, Y. Liang, K. Li, Y. Zhu, S. Liu, R. Xu and W. Zhous, Design of 3D flowerlike $BiOCl_xBr_{1-x}$ nanostructure with high surface area for visible light photocatalytic activities, *J. Alloys Compd.*, 2017, **725**, 1144–1157.
85 S. Lu, J. Li, F. Duan, L. Duan, M. Du and M. Chen, One-step preparation of $Bi_4O_5Br_xI_{2-x}$ solid solution with superior photocatalytic performance for organic pollutants degradation under visible light, *Appl. Surf. Sci.*, 2019, **475**, 577–586.
86 S. Meng, Y. Bi, T. Yan, Y. Zhang, T. Wu, Y. Shao, D. Wei and B. Du, Room-temperature fabrication of bismuth oxybromide/oxyiodide photocatalyst and efficient degradation of phenolic pollutants under visible light, *J. Hazard. Mater.*, 2018, **358**, 20–32.
87 Y. Bai, X. Shi, P. Wang, L. Wang, H. Xie, Z. Li, L. Qu and L. Ye, Synthesis of one-dimensional $Bi_5O_7Br_{0.5}I_{0.5}$ solid solution for effective real oilfield wastewater treatment via exciton photocatalytic process, *J. Taiwan Inst. Chem. Eng.*, 2018, **91**, 358–368.
88 Z. Liu, J. Niu, P. Feng and Y. Zhu, Solvothermal synthesis of $Bi_{24}O_{31}Cl_xBr_{10-x}$ solid solutions with enhanced visible light photocatalytic property, *Ceram. Int.*, 2015, **41**(3), 4608–4615.
89 Y. D. Sun, C. Zeng, X. Zhang, Z. Q. Zhang, B. Yang and S. Q. Guo, Tendencies of alloyed engineering in BiOX-based photocatalysts: a state-of-the-art review, *Rare Met.*, 2024, **43**, 1488–1512.
90 J. Xie, Y. Cao, D. Jia and Y. Li, Dahlia-shaped $BiOCl_xI_{1-x}$ structures prepared by a facile solid-state method: Evidence and mechanism of improved photocatalytic degradation of rhodamine B dye, *J. Colloid Interface Sci.*, 2017, **503**(5), 115–123.
91 A. Al-Keisy, R. Mahdi, D. Ahmed, K. Al-Attafi and W. H. Wan, Enhanced Photoreduction Activity in $BiOI_{1-x}F_x$ Nanosheet for Efficient Removal of Pollutants from Aqueous Solution, *ChemistrySelect*, 2020, **5**, 9758–9764.
92 L. Zhang, F. Liu, X. Xiao, X. Zuo and J. Nan, Microwave synthesis of iodine-doped bismuth oxychloride microspheres for the visible light photocatalytic removal of toxic hydroxyl-contained intermediates of parabens: catalyst synthesis, characterization, and mechanism insight, *Environ. Sci. Pollut. Res.*, 2019, **26**(28), 28871–28883.
93 H. Guo, S. Wang, L. Li, Y. Zhang, W. Wang and Q. Sun, Facile fabrication of $BiOBr_xCl_{1-x}$ hierarchical microspheres photocatalysts for efficient degradation of diverse pollutants under visible light, *J. Mol. Struct.*, 2022, **1265**, 133359.
94 H. Y. Xu, X. Han, Q. Tan, K. J. Wu and S. Y. Qi, Crystal-chemistry insight into the photocatalytic activity of $BiOCl_xBr_{1-x}$ nanoplate solid solutions, *Front. Mater. Sci.*, 2017, **11**(2), 120–129.
95 Z. Jia, F. Wang, F. Xin and B. Zhang, Simple solvothermal routes to synthesize 3D $BiOBr_xI_{1-x}$ microspheres and their visible-light-induced photocatalytic properties, *Ind. Eng. Chem. Res.*, 2011, **50**(11), 6688–6694.
96 X. Wang, W. Bi, P. Zhai, X. Wang, H. Li, G. Mailhot and W. Dong, Adsorption and photocatalytic degradation of pharmaceuticals by $BiOCl_xI_y$ nanospheres in aqueous solution, *Appl. Surf. Sci.*, 2016, **360**, 240–251.
97 H. Huang, X. Li, X. Han, N. Tian, Y. Zhang and T. Zhang, Moderate band-gap-broadening induced high separation of electron–hole pairs in Br substituted BiOI: a combined experimental and theoretical investigation, *Phys. Chem. Chem. Phys.*, 2015, **17**, 3673–3679.
98 X. Ren, J. Li, X. Cao, B. Wang, Y. Zhang and Y. Wei, Synergistic effect of internal electric field and oxygen vacancy on the photocatalytic activity of $BiOBr_xI_{1-x}$ with isomorphous fluorine substitution, *J. Colloid Interface Sci.*, 2019, **554**, 500–511.
99 B. Yin and C. Liu, Convenient Synthesis and Enhanced Photocatalytic Activity of BiOI/BiOBr Nanostructures with Different Morphologies, *J. Nanosci. Nanotechnol.*, 2017, **18**(7), 4771–4779.
100 Z. Zhang, Y. Zhao, J. Shen, Z. Pan, Y. Guo, P. K. Wong and H. Yu, Synthesis of 1D $Bi_{12}O_{17}Cl_xBr_{2-x}$ nanotube solid solutions with rich oxygen vacancies for highly efficient removal of organic pollutants under visible light, *Appl. Catal., B*, 2020, **269**, 118774.
101 B. Luo, G. Liu and L. Wang, Recent advances in 2D materials for photocatalysis, *Nanoscale*, 2016, **8**, 6904–6920.

102 B. Zhang, J. Zhang, R. Duan, Q. Wan and X. Tan, Nano Energy BiOCl nanosheets with periodic nanochannels for high-efficiency photooxidation, *Nano Energy*, 2020, **78**, 105340.

103 J. Fortner, L. Yang and P. Banerjee, Highly Conducting, n-Type $Bi_{12}O_{15}C_{l6}$ Nanosheets with Superlattice- like Structure, *Chem. Mater.*, 2015, **27**, 7710–7718.

104 L. N. Thi, H. Tran Huu, T. N. Ngoc, N. S. M. Viswanath, H. T. T. Le, T. T. T. Phan, L. T. Nguyen, Q. T. H. Ta, H. L. Han, L. N. Tan and V. Vo, $BiOCl_{1-x}Br_x$ solid solution – Novel synthesis, highly-efficient visible-light-driven photocatalyst, and DFT study, *J. Alloys Compd.*, 2023, **960**, 170503.

105 X. Li, T. Chen, H. Lin, J. Cao, H. Huang and S. Chen, Intensive photocatalytic activity enhancement of Bi_5O_7I via coupling with band structure and content adjustable $BiOBr_xI_{1-x}$, *Sci. Bull.*, 2018, **63**(4), 219–227.

106 X. Qiu, S. Lin, J. Li and L. Guo, One-Step Coprecipitation Synthesis of $BiOCl_xBr_{1-x}$ Photocatalysts Decorated with CQDs at Room Temperature with Enhanced Visible-Light Response, *Inorg. Chem.*, 2022, **61**(28), 10999–11010.

107 C. Hua, X. Dong, Y. Wang, N. Zheng, H. Ma and X. Zhang, Synthesis of a $BiOCl_{1-x}Br_x$@AgBr heterostructure with enhanced photocatalytic activity under visible light, *RSC Adv.*, 2018, **8**(30), 16513–16520.

108 B. Zhang, S. Fu, D. Wang, S. Jiao, Z. Zeng, X. Zhang, Z. Xu, Y. Liu, C. Zhao, J. Pan, D. Liu and J. Wang, Synthesis and enhanced light photocatalytic activity of modulating band $BiOBr_xI_{1-x}$ nanosheets, *Nanomaterials*, 2021, **11**(11), 2940.

109 J. Wan, W. Yang, J. Liu, K. Sun, L. Liu and F. Fu, Enhancing an internal electric field by a solid solution strategy for steering bulk-charge flow and boosting photocatalytic activity of $Bi_{24}O_{31}Cl_xBr_{10-x}$, *Chin. J. Catal.*, 2022, **43**(2), 485–496.

110 X. Zhang, L. W. Wang, C. Y. Wang, W. K. Wang, Y. L. Chen, Y. X. Huang, W. W. Li, Y. J. Feng and H. Q. Yu, Synthesis of $BiOCl_xBr_{1-x}$ Nanoplate Solid Solutions as a Robust Photocatalyst with Tunable Band Structure, *Chem. – Eur. J.*, 2015, **21**(33), 11872–11877.

111 Y. L. Qi, Y. F. Zheng and X. C. Song, Au-$BiOCl_{1-x}Br_x$ composites with highly enhanced photocatalytic activity for phenol decomposition, *J. Alloys Compd.*, 2017, **726**, 1147–1154.

112 J. Han, G. Zhu, M. Hojamberdiev, J. Peng and P. Liu, Temperature effect on phase transition and morphological transformation of BiOI microspheres to Bi_5O_7I microstructures, *Mater. Lett.*, 2016, **169**, 122–125.

113 L. Zhang, J. Yang, X. Zhao, X. Xiao, F. Sun, X. Zuo and J. Nan, Small-molecule surface-modified bismuth-based semiconductors as a new class of visible-light-driven photocatalytic materials: Structure-dependent photocatalytic properties and photosensitization mechanism, *Chem. Eng. J.*, 2020, **380**, 122546.

114 L. Chen, S. F. Yin, R. Huang, Y. Zhou, S. L. Luo and C. T. Au, Facile synthesis of BiOCl nano-flowers of narrow band gap and their visible-light-induced photocatalytic property, *Catal. Commun.*, 2012, **23**, 54–57.

115 J. Zhang, Q. Han, J. Zhu and X. Wang, A facile and rapid room-temperature route to hierarchical bismuth oxyhalide solid solutions with composition-dependent photocatalytic activity, *J. Colloid Interface Sci.*, 2016, **477**, 25–33.

116 M. Yadav, S. Garg, A. Chandra and K. Hernadi, Fabrication of leaf extract mediated bismuth oxybromide/oxyiodide ($BiOBr_xI_{1-x}$) photocatalysts with tunable band gap and enhanced optical absorption for degradation of organic pollutants, *J. Colloid Interface Sci.*, 2019, **555**, 304–314.

117 Y. L. Qi, Y. F. Zheng and X. C. Song, Synthetic adjustable energy band structure of $BiPO_4$-$BiOCl_xBr_{1-x}$ p–n heterojunctions with excellent photocatalytic activity, *J. Taiwan Inst. Chem. Eng.*, 2017, **77**, 216–226.

118 L. Qi, Y. Yang, P. Zhang, Y. Le, C. Wang and T. Wu, Hierarchical flower-like $BiOI_xBr_{(1-x)}$ solid solution spheres with enhanced visible-light photocatalytic activity, *Appl. Surf. Sci.*, 2019, **467–468**, 792–801.

119 X. Sun, Y. Zhang, C. Li, Z. Zhang, Z. Peng, H. Si and L. Y. Zhang, $BiOCl_xBr_yI_z$ (x + y + z = 1) solid solutions with controllable band gap and highly enhanced visible light photocatalytic performances, *J. Alloys Compd.*, 2015, **638**, 254–260.

120 Y. Zhang, X. Sun, G. Yang, Y. Zhu, H. Si, J. Zhang and Y. Li, Preparation and characterization of bifunctional $BiOCl_xI_y$ solid solutions with excellent adsorption and photocatalytic abilities for removal of organic dyes, *Mater. Sci. Semicond. Process.*, 2015, **41**, 193–199.

121 H. Wang, B. Zhang, F. Zhao and B. Zeng, One-Pot Synthesis of N-Graphene Quantum Dot-Functionalized I-BiOCl Z-Scheme Cathodic Materials for "signal-Off" Photoelectrochemical Sensing of Chlorpyrifos, *ACS Appl. Mater. Interfaces*, 2018, **10**(41), 35281–35288.

122 A. M. Alansi, T. F. Qahtan, N. Al Abass, M. Al-Qunaibit and T. A. Saleh, In-situ sunlight-driven tuning of photo-induced electron-hole generation and separation rates in bismuth oxychlorobromide for highly efficient water decontamination under visible light irradiation, *J. Colloid Interface Sci.*, 2022, **614**, 58–65.

123 Q. Zhang, W. Nie, T. Hou, H. Shen, Q. Li, C. Guan, L. Duan and X. Zhao, Optical and Photocatalytic Properties of Br-Doped BiOCl Nanosheets with Rich Oxygen Vacancies and Dominating {001} Facets, *Nanomaterials*, 2022, **12**(14), 2423.

124 G. Zhang, L. Cai, Y. Zhang and Y. Wei, Bi^{5+}, $Bi^{(3-x)+}$, and Oxygen Vacancy Induced $BiOCl_xI_{1-x}$ Solid Solution toward Promoting Visible-Light Driven Photocatalytic Activity, *Chem. – Eur. J.*, 2018, **24**(29), 7434–7444.

125 M. Ji, Y. Shao, E. Nkudede, Z. Liu, X. Sun, J. Zhao, Z. Chen, S. Yin, H. Li and J. Xia, Oxygen vacancy triggering the broad-spectrum photocatalysis of bismuth oxyhalide solid solution for ciprofloxacin removal, *J. Colloid Interface Sci.*, 2022, **626**, 221–230.

126 K. Xu, D. Xu, Z. Li, S. Zhang, L. Tong, J. Peng, S. Zhang, J. Shen and X. Chen, Enhanced visible-light photocatalytic degradation of ciprofloxacin hydrochloride by bulk iodine doped BiOCl with rich oxygen vacancy, *Appl. Surf. Sci.*, 2022, **578**, 152083.

127 H. Wang, B. Zhang, J. Xi, F. Zhao and B. Zeng, Z-scheme I-BiOCl/CdS with abundant oxygen vacancies as highly

effective cathodic material for photocathodic immunoassay, *Biosens. Bioelectron.*, 2019, **141**(6), 111443.

128 J. Guo, X. Li, J. Liang, X. Yuan, L. Jiang, H. Yu, H. Sun, Z. Zhu, S. Ye, N. Tang and J. Zhang, Fabrication and regulation of vacancy-mediated bismuth oxyhalide towards photocatalytic application: Development status and tendency, *Coord. Chem. Rev.*, 2021, **443**, 214033.

129 C. Wang, H. Qiu, T. Inoue and Q. Yao, Electronic structure calculations of I and Mn doped BiOCl with modified Becke – Johnson potential, *Comput. Mater. Sci.*, 2014, **85**, 138–141.

130 H. Liu, Y. Su, Z. Chen, Z. Jin and Y. Wang, Novel 3D flowerlike Au/$BiOBr_{0.2}I_{0.8}$ composites with highly enhanced visible-light photocatalytic performances, *Sep. Purif. Technol.*, 2014, **133**, 343–350.

131 Z. Han, M. Lv, X. Shi, G. Li, J. Zhao and X. Zhao, Regulating the Electronic Structure of Fe^{3+}-Doped $BiOCl_xI_{1-x}$ Solid Solution by an Amidoxime-Functionalized Fibrous Support for Efficient Photocatalysis, *Adv. Fiber Mater.*, 2023, **5**(1), 266–281.

132 S. S. Cui, X. Liu, Y. B. Shi, M. Y. Ding and X. F. Yang, Construction of atomic-level charge transfer channel in $Bi_{12}O_{17}C_{l2}$/MXene heterojunctions for improved visible-light photocatalytic performance, *Rare Met.*, 2022, **41**(7), 2405–2416.

133 C. Zeng, Y. Hu and H. Huang, $BiOBr_{0.75}I_{0.25}/BiOIO_3$ as a Novel Heterojunctional Photocatalyst with Superior Visible-Light-Driven Photocatalytic Activity in Removing Diverse Industrial Pollutants, *ACS Sustainable Chem. Eng.*, 2017, **5**(5), 3897–3905.

134 D. Wu, L. Zeng, Y. Liu, C. Yuan, X. Xue and X. Zhang, Design of 2D/2D heterojunction of $Ti_3C_2/BiOCl_xBr_{1-x}$ for enhancing photocatalytic performance, *Colloids Surf., A*, 2023, **663**, 131010.

135 J. Han, C. Lu, Y. Wang, S. Zhang, L. Zhang and Q. Yin, Fabrication of TiO_2-$BiOBr_xI_{1-x}$ heterojunctions with adjustable band structure for enhanced visible light photocatalytic activity, *J. Alloys Compd.*, 2020, **825**, 152047.

136 P. Yue, G. Zhang, X. Cao, B. Wang, Y. Zhang and Y. Wei, In situ synthesis of Z-scheme $BiPO_4/BiOCl_{0.9}I_{0.1}$ heterostructure with multiple vacancies and valence for efficient photocatalytic degradation of organic pollutant, *Sep. Purif. Technol.*, 2019, **213**, 34–44.

137 L. Zhang, Y. Li, Q. Li, J. Fan, S. A. C. Carabineiro and K. Lv, Recent advances on Bismuth-based Photocatalysts: Strategies and mechanisms, *Chem. Eng. J.*, 2021, **419**, 129484.

138 S. Shi, M. A. Gondal, S. G. Rashid, Q. Qi, A. A. Al-saadi, Z. H. Yamani, Y. Sui, Q. Xu and K. Shen, Synthesis of g-$C_3N_4/BiOCl_xBr_{1-x}$ hybrid photocatalysts and the photoactivity enhancement driven by visible light, *Colloids Surf., A*, 2014, **461**, 202–211.

139 X. Hu, Y. Zhang, B. Wang, H. Li and W. Dong, Novel g-$C_3N_4/BiOCl_xI_{1-x}$ nanosheets with rich oxygen vacancies for enhanced photocatalytic degradation of organic contaminants under visible and simulated solar light, *Appl. Catal., B*, 2019, **256**, 117789.

140 X. Sun, Y. Du, Z. Li, S. Chen, Y. Feng, N. Jiang, Y. Liu, J. Wang and H. Li, Facile synthesis of g-$C_3N_4/BiOCl_xI_{1-x}$ hybrids with efficient charge separation for visible-light photocatalysis, *Ceram. Int.*, 2020, **46**, 10843–10850.

141 Y. Feng, Y. Du, M. Du, Z. Li, Z. He, K. Yang, X. Lv, N. Jiang and Y. Liu, Facile constructing novel 3D porous g-$C_3N_4/BiOBr_{0.2}I_{0.8}$ hybrids: Efficient charge separation for visible-light photocatalysis, *J. Alloys Compd.*, 2018, **767**, 241–252.

142 H. Liu, Y. Su, Z. Chen, Z. Jin and Y. Wang, Graphene sheets grafted three-dimensional $BiOBr_{0.2}I_{0.8}$ microspheres with excellent photocatalytic activity under visible light, *J. Hazard. Mater.*, 2014, **266**, 75–83.

143 K. Gao, X. Gao, W. Zhu, C. Wang, T. Yan, F. Fu, J. Liu, C. Liang and Q. Li, The hierarchical layered microsphere of $BiOI_xBr_{1-x}$ solid solution decorated with N-doped CQDs with enhanced visible light photocatalytic oxidation pollutants, *Chem. Eng. J.*, 2021, **406**, 127155.

144 J. Han, S. Zhang, C. Lu, L. Zhang, K. Cao, N. Li and Q. Yin, Band engineering design of g-C_3N_4-$BiOCl_xBr_{1-x}$ direct Z-scheme heterojunctions with remarkable enhancement of photocatalytic performance, *Appl. Surf. Sci.*, 2021, **546**, 148887.

145 W. Dong, H. Ren, T. Xie and H. Lin, A novel route to synthesize $BiOCl_{1-x}Br_x$ solid solution with excellent photocatalytic performance in visible range by etching bismuth glass, *Mater. Lett.*, 2022, **317**, 132043.

146 M. Yadav, S. Garg, A. Chandra and K. Hernadi, Fabrication of leaf extract mediated bismuth oxybromide/oxyiodide ($BiOBr_xI_{1-x}$) photocatalysts with tunable band gap and enhanced optical absorption for degradation of organic pollutants, *J. Colloid Interface Sci.*, 2019, **555**, 304–314.

147 F. Deng, Y. Luo, H. Li, B. Xia, X. Luo, S. Luo and D. D. Dionysiou, Efficient toxicity elimination of aqueous Cr(VI) by positively-charged $BiOCl_xI_{1-x}$, $BiOBr_xI_{1-x}$ and $BiOCl_xBr_{1-x}$ solid solution with internal hole-scavenging capacity via the synergy of adsorption and photocatalytic reduction, *J. Hazard. Mater.*, 2020, **383**, 121127.

148 Y. Bai, L. Ye, T. Chen, P. Wang, L. Wang, X. Shi and P. K. Wong, Synthesis of hierarchical bismuth-rich $Bi_4O_5Br_xI_{2-x}$ solid solutions for enhanced photocatalytic activities of CO_2 conversion and Cr(VI) reduction under visible light, *Appl. Catal., B*, 2017, **203**, 633–640.

149 H. Ji, C. Hu, S. Zhang, L. Zhang and X. Yang, $BiO(OH)_xI_{1-x}$ solid solution with rich oxygen vacancies: interlayer guest hydroxyl for improved photocatalytic properties, *J. Colloid Interface Sci.*, 2022, **605**, 1–12.

150 A. Chachvalvutikul, T. Luangwanta, B. Inceesungvorn and S. Kaowphong, Bismuth-rich oxyhalide ($Bi_7O_9I_3$–$Bi_4O_5Br_2$) solid-solution photocatalysts for the degradation of phenolic compounds under visible light, *J. Colloid Interface Sci.*, 2023, **641**, 595–609.

151 X. Wang, Z. Zhang, Y. Xue, M. Nie, H. Li and W. Dong, Low crystallized $BiOCl_{0.75}I_{0.25}$ synthesized in mixed solvent and its photocatalytic properties under simulated solar irradiation, *Mater. Lett.*, 2014, **136**(3), 30–33.

152 C. S. L. Fung, M. Khan, A. Kumar and I. M. C. Lo, Visible-light-driven photocatalytic removal of PPCPs using magnetically separable bismuth oxybromo-iodide solid solutions: Mechanisms, pathways, and reusability in real sewage, *Sep. Purif. Technol.*, 2019, **216**, 102–114.

153 R. Lu, A. H. Zahid and Q. Han, Insight into the photocatalytic mechanism of the optimal x value in the $BiOBr_xI_{1-x}$, $BiOCl_xI_{1-x}$ and $BiOCl_xBr_{1-x}$ series varying with pollutant type, *Nanoscale*, 2022, **14**(37), 13711–13721.

154 X. Li, J. Cai, M. Li, L. Zhang and Z. Chen, Growth of $BiOBr_xI_{1-x}$ solid-solutions with tunable band-gaps on carbon fiber cloth as flexible membrane-shaped photocatalyst for purifying antibiotic wastewater, *J. Cleaner Prod.*, 2023, **414**, 137725.

155 T. Kaewmanee, S. Wannapop, A. Phuruangrat, T. Thongtem and S. Thongtem, Solvothermal synthesis of $BiOBr_xI_{1-x}$ (x = 0.0–1.0) solid solutions used for adsorption and photodegradation of cationic and anionic dyes, *Inorg. Chem. Commun.*, 2021, **134**, 109054.

156 H. Y. Xu, D. Lu, Q. Tan, X. L. He and S. Y. Qi, Visible-light-driven photocatalytic degradation of rhodamine B in water by $BiOCl_xI_{1-x}$ solid solutions, *Water Sci. Technol.*, 2020, **81**(5), 1080–1089.

157 L. Kong, J. Guo, J. W. Makepeace, T. Xiao, H. F. Greer, W. Zhou, Z. Jiang and P. P. Edwards, Rapid synthesis of $BiOBr_xI_{1-x}$ photocatalysts: Insights to the visible-light photocatalytic activity and strong deviation from Vegard's law, *Catal. Today*, 2019, **335**, 477–484.

158 S. Liu, P. Liang, J. Liu, J. Xin, X. Li, C. Shao, X. Li and Y. Liu, Anchoring bismuth oxybromo-iodide solid solutions on flexible electrospun polyacrylonitrile nanofiber mats for floating photocatalysis, *J. Colloid Interface Sci.*, 2022, **608**, 3178–3191.

159 J. Lu, Q. Meng, H. Lv, L. Shui, M. Jin, Z. Zhang, Z. Chen, M. Yuan, X. Wang, J. M. Liu and G. Zhou, Synthesis of visible-light-driven $BiOBr_xI_{1-x}$ solid solution nanoplates by ultrasound-assisted hydrolysis method with tunable bandgap and superior photocatalytic activity, *J. Alloys Compd.*, 2018, **732**, 167–177.

160 K. Ren, J. Liu, J. Liang, K. Zhang, X. Zheng, H. Luo, Y. Huang, P. Liu and X. Yu, Synthesis of the bismuth oxyhalide solid solutions with tunable band gap and photocatalytic activities, *Dalton Trans.*, 2013, **42**(26), 9706–9712.

161 D. Du, W. Li, S. Chen, T. Yan, J. You and D. Kong, Synergistic degradation of rhodamine B on $BiOCl_xBr_{1-x}$ sheets by combined photosensitization and photocatalysis under visible light irradiation, *New J. Chem.*, 2015, **39**(4), 3129–3136.

162 H. Gnayem, A. Dandapat and Y. Sasson, Development of Hybrid $BiOCl_xBr_{1-x}$-Embedded Alumina Films and Their Application as Highly Efficient Visible-Light-Driven Photocatalytic Reactors, *Chem. – Eur. J.*, 2016, **22**(1), 370–375.

163 Y. y. Gu, Y. q. Xiong, X. x. Zhang, L. Zhao, S. c. Zhang and J. Yan, Facile synthesis of hierarchical $BiOCl_xBr_{1-x}$ solid solution with enhanced photocatalytic activity, *J. Cent. South Univ.*, 2018, **25**(7), 1619–1627.

164 X. Zhang, C. Y. Wang, L. W. Wang, G. X. Huang, W. K. Wang and H. Q. Yu, Fabrication of $BiOBr_xI_{1-x}$ photocatalysts with tunable visible light catalytic activity by modulating band structures, *Sci. Rep.*, 2016, **6**, 22800.

165 S. Shenawi-Khalil, V. Uvarov, Y. Kritsman, E. Menes, I. Popov and Y. Sasson, A new family of $BiO(Cl_xBr_{1-x})$ visible light sensitive photocatalysts, *Catal. Commun.*, 2011, **12**(12), 1136–1141.

166 G. Zhang, L. Zhang, Y. Liu, L. Liu, C. P. Huang, H. Liu and J. Li, Substitution Boosts Charge Separation for High Solar-Driven Photocatalytic Performance, *ACS Appl. Mater. Interfaces*, 2016, **8**(40), 26783–26793.

167 N. Mohseni, M. Haghighi and M. Shabani, Sunlight-activated 3D-mesoporous-flowerlike Cl–Br bismuth oxides nanosheet solid solution: In situ EG-thermal-sonication synthesis with excellent photodecomposition of ciprofloxacin, *Environ. Res.*, 2020, **188**, 109810.

168 Y. Li, J. Lai, X. Zheng, S. Lv, J. Yang and S. Cui, Fabrication of wool ball-like F-doped $BiOCl_{0.4}Br_{0.3}I_{0.3}$ composite for effective sulfamethazine photocatalytic degradation, *Mater. Res. Bull.*, 2020, **130**, 110937.

169 S. Gholizadeh and M. Haghighi, Environmental Facile one-pot ultrasound-assisted solvothermal fabrication of ball- flowerlike nanostructured $(BiOBr)_x(Bi_7O_9I_3)$1-x solid-solution for high active photodegradation of antibiotic levofloxacin under sunlight, *Appl. Catal., B*, 2019, **248**, 320–331.

170 R. Ameta, S. Benjamin, A. Ameta and S. C. Ameta, Photocatalytic degradation of organic pollutants: A review, *Mater. Sci. Forum*, 2013, **734**, 247–272.

171 X. Gao, K. Gao, W. Zhu, C. Liang, Q. Li, F. Fu and Y. Zhu, Accurate guided alternating atomic layer enhance internal electric field to steering photogenerated charge separation for enhance photocatalytic activity, *Appl. Catal., B*, 2021, **298**, 120536.

172 Q. Y. Liu, G. Han, Y. F. Zheng and X. C. Song, Synthesis of $BiOBr_xI_{1-x}$ solid solutions with dominant exposed {0 0 1} and {1 1 0} facets and their visible-light-induced photocatalytic properties, *Sep. Purif. Technol.*, 2018, **203**, 75–83.

173 H. He, C. Liu, M. Li, Y. Liu and R. Zhu, Synergistic photocatalytic degradation mechanism of $BiOCl_xI_{1-x}$-OVs based on oxygen vacancies and internal electric field-mediated solid solution, *Chemosphere*, 2023, **337**, 139281.

174 X. Zhang, P. Yang, B. Yang, Y. Bai, W. Liu and K. Zhang, Synthesis of the $Ag\text{-}AgCl_{0.5}Br_{0.5}/BiOCl_{0.5}Br_{0.5}$ composite for enhanced photocatalytic activity of degradation of oil field pollutant through synergistic effect of ag-bi based solid solution, *J. Photochem. Photobiol., A*, 2019, **384**, 112047.

175 X. Zhang, P. Yang, Y. Bai, B. Yang and W. Liu, Synthesis of efficient composite photocatalysts from solid solution $B_{i3}O_4Cl_{0.5}Br_{0.5}$ and Ag-AgI/AgCl for decomposition the oil field pollutants of phenol and acrylamide, *Adv. Powder Technol.*, 2020, **31**(3), 973–985.

176 Q. Qin, Y. Guo, D. Zhou, Y. Yang and Y. Guo, Facile growth and composition-dependent photocatalytic activity of flowerlike $BiOCl_{1-x}Br_x$ hierarchical microspheres, *Appl. Surf. Sci.*, 2016, **390**, 765–777.

177 H. Zhang, J. C. L. Tee, S. Jaenicke, M. A. Gondal, M. A. Dastageer, C. Basheer and G. K. Chuah, $BiOBr_nI_{1-n}$ solid solutions as versatile photooxidation catalysts for phenolics and endocrine disrupting chemicals, *Catal. Today*, 2021, **375**, 547–557.

178 M. B. Hussain, M. S. Khan, H. M. Loussala and M. S. Bashir, The synthesis of a $BiOCl_xBr_{1-x}$ nanostructure photocatalyst with high surface area for the enhanced visible-light photocatalytic reduction of Cr(VI), *RSC Adv.*, 2020, **10**(8), 4763–4771.

179 J. Wang, H. Mei, D. Jin, Q. Lin, R. Zhang and X. Wang, Indirect Substitution Constructing Halogen-Vacancy $BiOCl_{1-x}I_n$ Solid Solution with a Suitable Surface Structure for Enhanced Photoredox Performance, *Inorg. Chem.*, 2022, **61**, 8540–8549.

180 X. Wu, K. Zhang, G. Zhang and S. Yin, Facile preparation of BiOX (X = Cl, Br, I) nanoparticles and up-conversion phosphors/BiOBr composites for efficient degradation of NO gas: Oxygen vacancy effect and near infrared light responsive mechanism, *Chem. Eng. J.*, 2017, **325**, 59–70.

181 F. Dong, Y. Sun, M. Fu, Z. Wu and S. C. Lee, Room temperature synthesis and highly enhanced visible light photocatalytic activity of porous BiOI/BiOCl composites nanoplates microflowers, *J. Hazard. Mater.*, 2012, **219–220**, 26–34.

182 T. Wu, X. Li, D. Zhang, F. Dong and S. Chen, Efficient visible light photocatalytic oxidation of NO with hierarchical nanostructured 3D flower-like $BiOCl_xBr_{1-x}$ solid solutions, *J. Alloys Compd.*, 2016, **671**, 318–327.

183 Y. Bai, P. Yang, P. Wang, Z. Fan, H. Xie, P. K. Wong and L. Ye, Solid phase fabrication of Bismuth-rich $Bi_3O_4Cl_xBr_{1-x}$ solid solution for enhanced photocatalytic NO removal under visible light, *J. Taiwan Inst. Chem. Eng.*, 2018, **82**, 273–280.

184 M. Ou, F. Dong, W. Zhang and Z. Wu, Efficient visible light photocatalytic oxidation of NO in air with band-gap tailored $(BiO)_2CO_3$-BiOI solid solutions, *Chem. Eng. J.*, 2014, **255**, 650–658.

185 M. Gao, J. Yang, T. Sun, Z. Zhang, D. Zhang, H. Huang, H. Lin, Y. Fang and X. Wang, Persian buttercup-like $BiOBr_x$-Cl_{1-x} solid solution for photocatalytic overall CO_2 reduction to CO and O_2, *Appl. Catal., B*, 2019, **243**, 734–740.

186 D. Pancholi, N. S. Bisht, V. Pande and A. Dandapat, Development of novel $BiOBr_{0.75}I_{0.25}$ nanostructures with remarkably High dark phase bactericidal activities, *Colloids Surf., B*, 2021, **199**, 111558.

187 A. Dandapat, I. Horovitz, H. Gnayem, Y. Sasson, D. Avisar, T. Luxbacher and H. Mamane, Solar Photocatalytic Degradation of Trace Organic Pollutants in Water by Bi(0)-Doped Bismuth Oxyhalide Thin Films, *ACS Omega*, 2018, **3**(9), 10858–10865.

188 S. Ge, D. Li, Y. Gao, J. Hou, J. Fu, W. Li, P. Li, C. Zhu, S. Guo and Z. Zheng, Dual control of surface oxygen vacancies and exposed facets onto $BiOCl_{0.95}Br_{0.05}$ sheets for enhancing photocatalytic degradation of sodium pentachlorophenate, *J. Alloys Compd.*, 2021, **871**, 159568.

189 H. Gnayem and Y. Sasson, Nanostructured 3D Sunflower-like Bismuth Doped $BiOCl_xBr_{1-x}$ Solid Solutions with Enhanced Visible Light Photocatalytic Activity as a Remarkably Efficient Technology for Water Purification, *J. Phys. Chem. C*, 2015, **119**(33), 19201–19209.